d Collection

Thesis for the Degree of Master of Science

Source parameters of the December 22, 2015 Iksan earthquake

by

Roungyi Kim

In Division of Earth Environmental System Science

(Major of Earth & Environmental Sciences),

The Graduate School,

Pukyong National University

February 2017

Source parameters of the December 22, 2015 Iksan earthquake
(2015년 12월 22일 익산지진의 지진원 요소)

Advisor: Prof. Tae-Seob Kang

by
Roungyi Kim

A thesis submitted in partial fulfillment of the requirements
for the degree of

Master of Science

In Division of Earth Environmental System Science
(Major of Earth & Environmental Sciences),
The Graduate School,
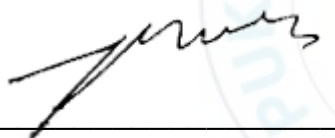Pukyong National University

February 2017

Source parameters of the December 22, 2015 Iksan earthquake
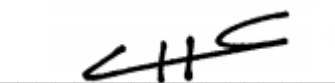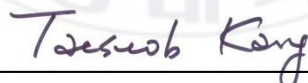
A dissertation

by

Roungyi Kim

Approved by:

_____

(Chairman) Young-Seog Kim

_____   _____

(Member) Hoseon Choi   (Member) Tae-Seob Kang

February 26, 2016

CONTENTS

i

List of Figures

iv

List of Tables

Source parameters of the December 22, 2015 Iksan earthquake

Roungyi Kim

Department of Earth Environmental System Science, The Graduate School,
Pukyong National University

Abstract

On December 22, 2015, an earthquake with M_L 3.9 occurred in the Iksan area (36.02°N, 126.95°E) of Jeonbuk. A series of earthquakes ($M_L < 2.0$) occurred three times after the Iksan earthquake. 1-D crustal velocity structure model of Kim, S. (Kim et al., 2011) for seismic analysis was consistently applied to determine location, depth, focal mechanism, and moment magnitude.

As a result of hypocenter relocation, there are almost no change in position. Analysis of most depth of relocation is distributed in 9 to 13km when the focal depth of the Korea Peninsula earthquake is around 10km(Lee, 2010). Result of HypoDD shows that there is no correlation with the surface faulting. The focal mechanism by the waveform inversion and P-wave first motion polarity analysis is that most events have thrust faulting. The compressional axes of the solutions are predominantly NE-SW in direction. This result is similar to the directions of principal compressional axes for major earthquakes occurred around South Korea (Cho *et al.*, 2006). The moment magnitude estimated by displacement spectral analysis was 3.9 ± 0.1, which is similar to that estimated by waveform inversion.

I Introduction

Most of the earthquakes on the South Korea are classified as a shallow earthquake inside the plate. In comparison with plate boundary seismicity, its scale is relatively small, its frequency is irregular, and its location is very sporadic (Cho *et al.*, 2006, Kim *et al.*, 2006a, Jun and Jeon, 2010). Established studies on earthquakes that occurred in the South Korea are mainly related thrust faulting, strike-slip faulting and strike-slip sense including partially thrust component. The principal compressive stresses that cause fault movement in seismic source is direction of ENE-WSW or NE-SW (Kim *et al.*, 2006b, Cho *et al.*, 2006, Park *et al.*, 2007, Jung and Kyung, 2013). In addition, studies on seismic source constants from past to present are underway. Generally, the internal plate stress drop is 100 Bar (Kanamori and Anderson, 1975). On the Korean Peninsula, where small or micro earthquakes with small moments are relatively frequent, they show a smaller stress drop value than earthquakes within the global plate (Jang, 2015). (Kim and Kim, 2008) obtained the source parameters on the Korean Peninsula and the surrounding area. The mean stress drop for the South Korea is about 1.0×10^{22} dyne-cm (M_L= 4.0). In this study was analysis source parameters of Iksan earthquakes on December 22, 2015. Iksan earth quakes that occurred on December 22, 2015 are located the western part of the Okchon Fold Belt in tectonic map of Korea (see Fig. 1), and belong to the GangGyong sheet and Hamyol sheet in geological map of Korea of the Korea Institute of Geoscience and Mineral Resources. Among the land earthquakes that occurred prior to the Gyeongju earthquakes in September 2016, the Iksan earthquake was the M_L 3.9 that is the relatively mid-sale earthquake. After the

1

M_L 3.9 event, an earthquake occurred three times in a row on December 22. In addition, this study analyzed source parameters of the earthquake on May 11, 2015 and the earthquake on February 9, 2016 that are close to the earthquakes on December 22, 2015.
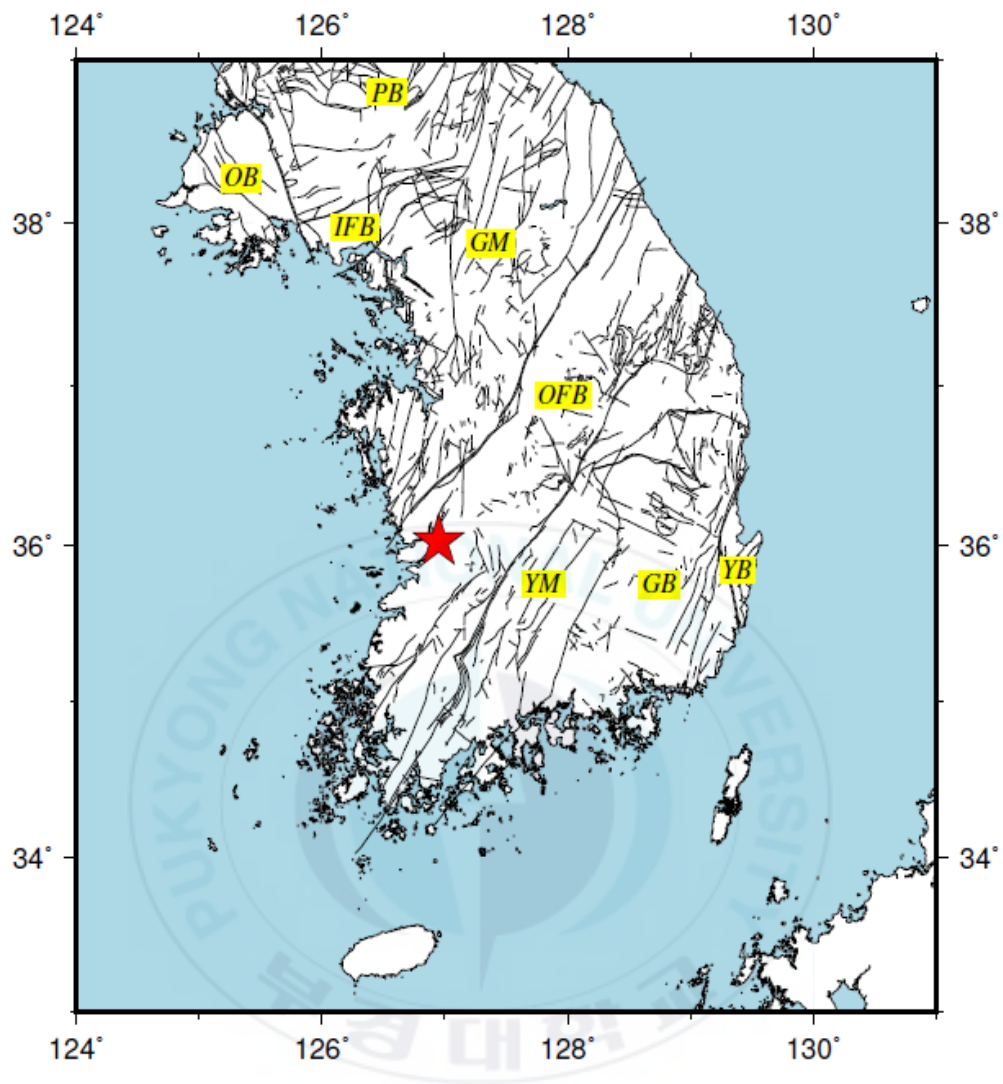
Figure 1 Position of this study located in the western part of the Okchon Fold Belt.

II Theory and Method

In addition to the magnitude 3.9 event on December 22, 2015, a series of earthquakes ($M_L < 2.0$) occurred three times. Tale 1 shows that the Iksan earthquake catalog published by National Seismic Information System (http://necis.kma.go.kr) of Korea Meteorological Administration (NECIS of KMA) and the Korea Institute of Geoscience and Mineral Resources (KIGAM). This study selected two events that relatively short-term of occurrence based on December 22, 2015 and added the Iksan earthquake catalog. For the Iksan earthquake location from 1996 to 2016, see Table 1 and Fig. 2.

The hypocenter relocation analysis and the focal mechanism by the P-wave first motion polarity analysis used velocity and acceleration records. But the focal mechanism by the waveform inversion used only broadband velocity records. This study applied the 1-D crustal velocity structure model of Kim, S. (Kim et al., 2011) consistently to all steps (see Fig 3). Figure 4 shows that a work flow chart from the seismic data acquisition to get source parameters.

1. Hypocenter Relocation

Source parameters is comprehensive concept that include the source's longitude, latitude, focal depth, focal mechanism, and origin time. It is an important factor for analyzing the characteristics of basic earthquake information. The determination of accurate inverted source parameters is sensitivity that waveform quality, seismic station distribution, velocity model, accuracy of inversion algorithm and the ray tracing between two points. Thus, the accuracy of the velocity model is important for correct

determination of source parameters. However, in the south of Korea Peninsula, there exist various velocity models that have not defined accurate, so making use of an approximate 1-D velocity model. Thus, the 1-D velocity models naturally get errors into the source parameters. An algorithm is needed by which accurate source parameters can be determined using an approximate 1-D velocity model(Kim *et al.*, 2014).

In this study, hypocentral relocation is performed by using the Velellipse program which finds the optimum 1-D velocity model with minimum root mean square(RMS) error. First, user determine a semi-optimum 1-D P and S velocity model (See Table 1). User prepare a set of P velocity models that are shifted by constant velocity from initial P velocity model:

$$\alpha_i^n = \alpha_i^0 \pm n\Delta\alpha, (n = 0,1,\cdots,N) \tag{1}$$

$\Delta\alpha$: constant velocity interval

n= integer varying from 0 to N

α_i^0= P velocity in the ith layer of initial velocity model

α_i^n= P velocity in the ith layer of the nth velocity model prepared

The S wave velocity models are calculated subsequently from a given Vp/Vs ratio and the P velocity model. After that the synthetic traveltimes of P and S waves are calculate for every velocity model, and the misfit error between the synthetic and observed trveltimes is calculated.

The following equation is the misfit error, F:

$$F = \frac{\sqrt{3\overline{\Delta t_p}^2 + \overline{\Delta t_s}^2}}{4} \qquad (2)$$

$\overline{\Delta t_p}$: Traveltime differences of P waves

$\overline{\Delta t_s}$: Traveltime differences of S waves

Equation (2), an optimum velocity model is selected which the error of the traveltime is minimized, that is, the error of the matching is minimized(Kim *et al.*, 2006b). The velocity model with the minimum misfit error is chosen as the optimum velocity model for a given velocity interval($\Delta\alpha$). It can be used as a new initial velocity model for improvement with the addition of velocity model and can be obtained by iterative implementation with a smaller $\Delta\alpha$ in equation (1). The velocity model with the minimum misfit error is finally considered as the optimal velocity model if the smallest $\Delta\alpha$ is realized. Therefore, source parameters are determined from the optimum velocity model that the traveltime difference is minimized by iterative calculation method.

HypoDD (Double-Difference Hypocenter Location) Software was performed to check that the result of distributed relocation is correlated with the fault on the surface. This is Fortran computer program package that re-determines the location of events according to algorithm of traveltime differences (Double -Difference, DD) between events. The software is calculated equation (3) that defines traveltime differences (Fréchet, 1985, Waldhauser and Ellsworth, 2000).

$$dr_k^{ij} = (t_k^i - t_k^j)^{obs} - (t_k^i - t_k^j)^{cal} \qquad (3)$$

dr_k^{ij}: residual between observed and calculated differential traveltime

i and j: event

k: seismic station

t: traveltime

Equation (3) can be shown that using the appropriate slowness vector and origin time term for each event (see Equation (4) and Fig. 5)

$$\frac{\partial t_k^i}{\partial m}\Delta m^i - \frac{\partial t_k^i}{\partial m}\Delta m^i = dr_k^{ij} \tag{4}$$

Where Δm is linearly related to perturbations and Δm^i is $(\Delta x^i, \Delta y^i, \Delta z^i, \Delta \tau^i)$ where τ^i is the origin time of event i.

The program uses the time difference information of the events pair at the seismic station common to each event as the basic data. Event relocation with hypoDD is a two-step process (see Fig. 6). The run files needed to calculate the double difference (DD) hypocenter locations are ph2dt and hypoDD. The ph2dt is used for the data preprocessing and then the output files use to run hypoDD in the event relocation process step. Ph2dt searches catalog P- and S-wave data for event pairs with traveltime information at common seismic stations and subsamples these data in order to optimize the quality of the wave pairs. HypoDD can determine the hypocenter position from the running DD technology(Waldhauser and Ellsworth, 2000, Waldhauser, 2001). The aim is to relocate events by combining all the available data.

2. Focal mechanism Analysis

Focal mechanism often called beach ball diagrams. It is commonly used way of graphically representing the fault geometry and slip direction of an earthquake. Figure 7 is examples of the simple cases of fault type. In general, focal mechanism is analyzed

by using P-wave first motion polarity analysis. However, there are disadvantages to applying this method to South of Korea. Seismic station randomly distributes. Comparing with plate boundary, small earthquakes occur relatively quite a lot in South of Korea. In the case of small earthquake (short-period earthquake) that include high frequency, the focal mechanism by using the P-wave first motion polarity is sensitive to velocity model. Namely, it is not easy to compute the accurate focal mechanism in the South of Korea that the correct velocity model is not defined. In order to overcome the disadvantages, in this study, focal mechanism by waveform inversion method was computed by using ISOLA software, and then focal mechanism result by waveform inversion verified by comparing the P-wave first polarity method.

ISOLA software calculates the focal mechanism, moment magnitude, seismic moment, and depth. ISOLA is based on multiple- or single- point source representation and iterative deconvolution method, similar to Kikuchi and Kanamori (1991) method for teleseismic data, but here the full wavefield is considered, and Green's functions are computed by using frequency-wavenumber method, such as, for example, the discrete wavenumber method of Bouchon (1981) and Cotton and Coutant (1997). Thus, the method can apply for regional and local distance. The retrieved point-source moment tensor (called subevents) is derived by the least squares method of the error between the synthetic- and observed waveform. Waveform inversion has to include grid search. The timing and position of the derived subevent is optimized through grid search(Sokos and Zahradnik, 2008, Sokos and Zahradník, 2013). The broadband velocity record is calibrated by using the instrument information file (called Pole-zero file) that includes the sensor and recorder information, and then instrumentally corrected band-pass

filtered velocity records are used. The code transforms velocity- into a displacement-waveform, inverts the displacement, and computes synthetic displacement.

It is assumed that the earthquake is caused by a fault, and the waveform is modeled by considering it as an earthquake source of Deviatoric component excluding the isotropic component. Allowing a relative time shift of the observed waveform(Sokos and Zahradnik, 2008, Choi and Shim, 2009, Choi, 2009, Choi, 2014).

ISOLA has been used the MATLAB-based interface (see Fig.8). Its purpose help user-friendly data handling of ISOLA-Fortran part with data preprocessing, Green function preparation, waveform inversion and display of the results. The source parameters are calculated using the variance reduction(VR) between the observed and synthetic waveforms using equation (5):

$$\text{VR} = 1 - \frac{\sum(d_i - s_i)^2}{\sum(d_i)^2} \times 100(\%) \tag{5}$$

In the equation (5), d_i is observed waveform and s_i is synthetic waveform.

The reliability of VR value is classified into the following grades.

-A, at least of three seismic stations have VR >80 %.

-B, one seismic station or two seismic stations should have VR= 70-80% or VR>80%.

-C, VR=60-70%.

-D, VR<60%, this value is uncertain.

FOCMEC (coded in Fortran 77) contains software for determining and displaying double-couple earthquake focal mechanisms. Input data are first polarities (P, SV, and SH), amplitude ratios (SV/P, SH/P and SV/SH), station identifiers, azimuths and takeoff

9

angles at the source. Focmec performs an efficient, systematic search of the focal sphere and reports acceptable solutions based on selection criteria for the number of polarity errors and errors in amplitude ratio (Snoke, 2003). But this study used only the first arrival P-wave polarities information. The focal mechanism solutions of the events in regions with well-decided velocity models can be determined using the first arrival P-wave polarities (see Fig. 9). However, the polarity based analysis is important that good azimuthal coverage for accurate determination of focal mechanism solution.

Earthquake faulting types for this study are investigated according to the method suggested by (Frohlich, 1992). This method is a triangle diagram to characterize focal mechanism solutions as strike-slip, normal or thrust faultings of the earthquake in terms of dip angles with respect to horizontal of their P, T, and B axes. Strike-slip and normal faulting earthquakes are defined as those having B and P dip angles (δ_B and δ_P) greater than $60°$and thrust faulting earthquakes are defined as those having T dip angle (δ_T) greater than $50°$. Mechanisms satisfying none of those standards are defined to be odd mechanism. Horizontal and Vertical location values, h and v of the triangle diagram based on δ_B, δ_P and δ_T are calculate as following equations (Frohlich, 1992):

$$h = \frac{\cos \delta_B \sin \varphi}{\sin \eta \sin \delta_B + \cos \eta \cos \delta_B \cos \varphi}$$

$$v = \frac{\cos \eta \sin \delta_B - \sin \eta \cos \delta_B \cos \varphi}{\sin \eta \sin \delta_B + \cos \eta \cos \delta_B \cos \varphi} \tag{6}$$

$$\varphi = \arcsin(\frac{\sin \delta_B}{\sin \delta_B}) - 45°$$

where η is $35.26°$, which is the dip angle of the P, T and B axes for the focal mechanism solution which plots in center of the diagram(Choi, 2012).

3. Spectrum Analysis

To confirm the reliability of moment magnitude which is one of the results of ISOLA, displacement amplitude spectral analysis calculated.

The displacement amplitude spectra can be calculated by multiplying the transfer equation (7):

$$A(R, f) = S(f) \cdot D(f) \cdot G(R) \cdot I(f) \cdot SE(f) \tag{7}$$

In equation (7), S is source term, D is unelastic attenuation term, G is geometrical attenuation term, I is instrumental transfer function term and SE is site defect term. The composite spectrum method computes amplitude spectra (Noh *et al.*, 2003, Choi, 2009). The three components spectrum, which is a vectorially combines three components of three components seismic data in the frequency domain. The method has the advantage of eliminating vector splitting in a single component and enhancing the shape of the Fourier spectrum. D (unelastic attenuation term) and G (geometrical attenuation term) are expressed by the following equation (8):

$$D(f) = e^{-\frac{\pi f}{vQ(f)}}, \ G(R) = \frac{1}{R^n} \tag{8}$$

In the equation (6), v is shear wave velocity and Q is attenuation characteristics of medium.(Kim *et al.*, 2002) model is used as the attenuation term. I (instrumental transfer function term) is used to recover the actual vibration by removing the seismic response function from the seismic data. SE shows the ground characteristics of each seismic station. SE value was fixed at one because there was no previous research. A time window is set to obtain the displacement amplitude spectrum of a section for approximately 200 seconds after the arrival times of S waves. The time window is long enough to include subsequent S wave groups. The grid search method (Choi *et al.*, 2004)

is used to determine the moment magnitude and corner frequency. This method has an advantage of finding the minimum that minimizes the error value of the moment magnitude and corner frequency in the whole section. The moment magnitude and corner frequency were determined to minimize the error in the following equation (9):

$$E = \left[\sum_i \left| a_{i,obs} - a_{i,synth} \right|^n \right]^{\frac{1}{n}} \tag{9}$$

Where $a_{i,obs}$ is displacement amplitude spectral of observed data, $a_{i,synth}$ is displacement amplitude spectral of model and n value is one. In this study, the displacement amplitude spectral of the $M_L 3.9$ Iksan earthquake was analyzed, through the grid search method calculated moment magnitude, corner frequency and stress drop.
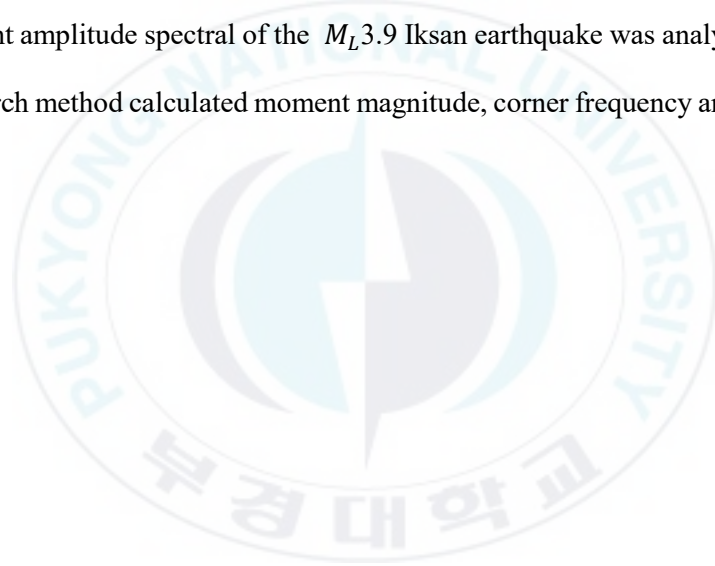
Table 1 The location of Iksan earthquakes was announced by the KMA and KIGAM from 1996 to 2016. Only the KIGAM provides information of focal depth.

Agency	Origin Time (KST)	Latitude ($^{\circ}N$)	Longitude ($^{\circ}E$)	Magnitude (M_L)	Depth (Km)
KMA	1996/06/21 01:04:08	36.1	126.9	2.8	-
KMA	1998/09/13 20:42:13	36.1	126.9	3.6	-
KMA	2005/06/02 22:30:26	36	126.98	1.3	-
KMA	2006/01/13 23:45:57	36.07	127.05	1.6	-
KMA	2006/02/04 23:18:05	36.08	127.03	1.4	-
KMA	2009/11/17 05:38:49	36.07	126.95	2.3	-
KMA	2010/03/26 04:07:30	36.09	127.04	1.1	-
KMA	2010/09/17 23:35:09	36.12	126.99	1.1	-
KMA	2010/10/20 01:14:35	35.96	126.97	1.2	-
KMA	2011/01/13 02:46:22	35.92	126.94	1.2	-

KMA	2012/09/29 21:03:47	35.99	126.5	1.1	-
KMA	2012/11/08 07:10:56	36.03	127.05	0.8	-
KMA	2012/11/08 07:32:01	36.03	127.05	1.1	-
KMA	2013/02/07 04:49:02	36.02	126.99	1.2	-
KMA	2015/05/11 03:39:25	36.05	126.95	1.2	-
KMA	2015/12/22 04:31:24	36.02	126.95	3.9	-
KIGAM	2015/12/22 04:31:25	36.03	126.9646	4.3	11.1
KMA	2015/12/22 05:02:47	36.02	126.96	0.8	-
KMA	2015/12/22 17:29:10	36.02	126.95	1.2	-
KMA	2015/12/22 21:20:58	36.03	126.96	1.7	-
KMA	2016/02/09 06:13:45	36.02	126.96	1.3	-

Table 2 The 1-D velocity model of (Kim *et al.*, 2011) derived using a full-grid search method.

Depth (Km)	Vp (Km/s)	Vs (Km/s)	Vp/Vs
0.0	5.63	3.39	1.66
7.3	6.17	3.61	1.71
20.7	6.58	3.70	1.78
31.3	7.77	4.44	1.75
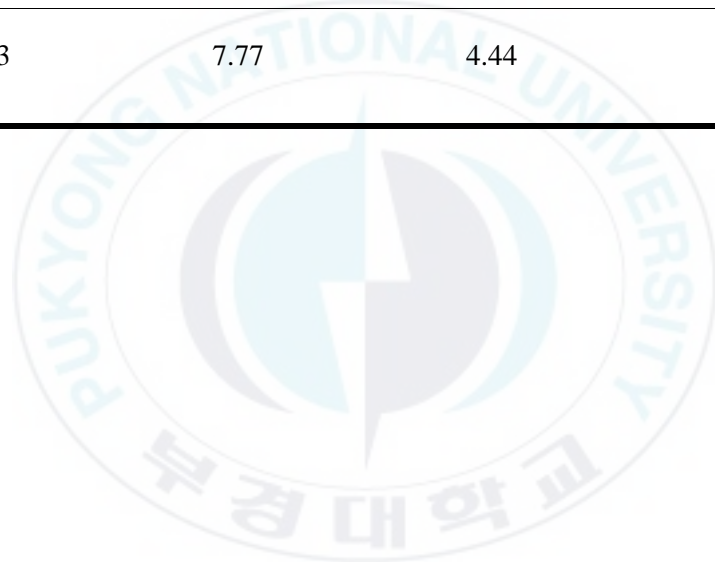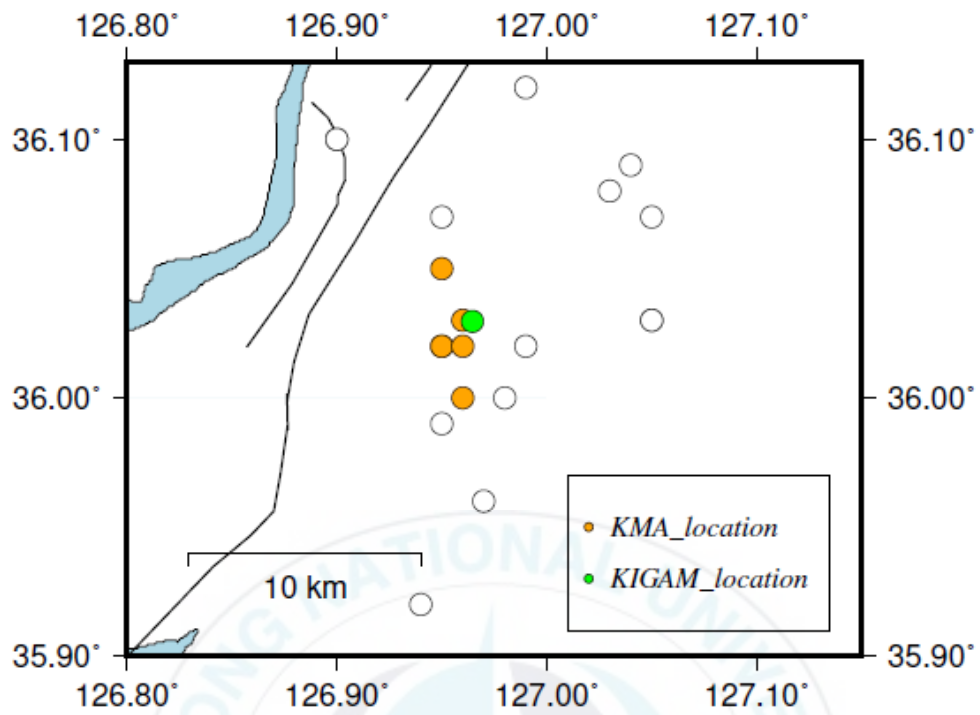
Figure 2 Circles show the position of earthquakes near Iksan from 1996 to 2016. The filled circles represent earthquakes analyzed in this study. Orange is the event location announced by the KMA and Green is the event location announced by the KIGAM.
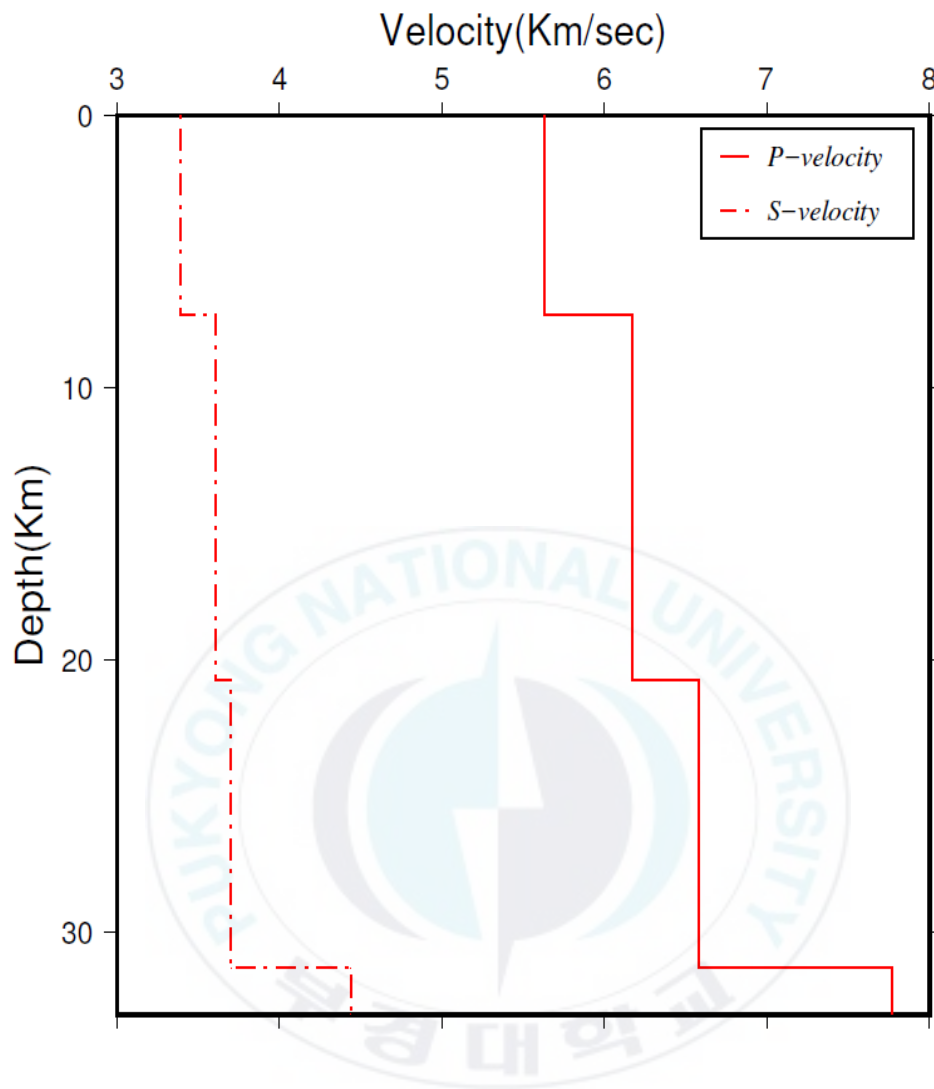
Figure 3 The 1-D velocity structure model applied to all processes of this study, the solid line shows the P wave velocity and the dashed line shows the S wave velocity.
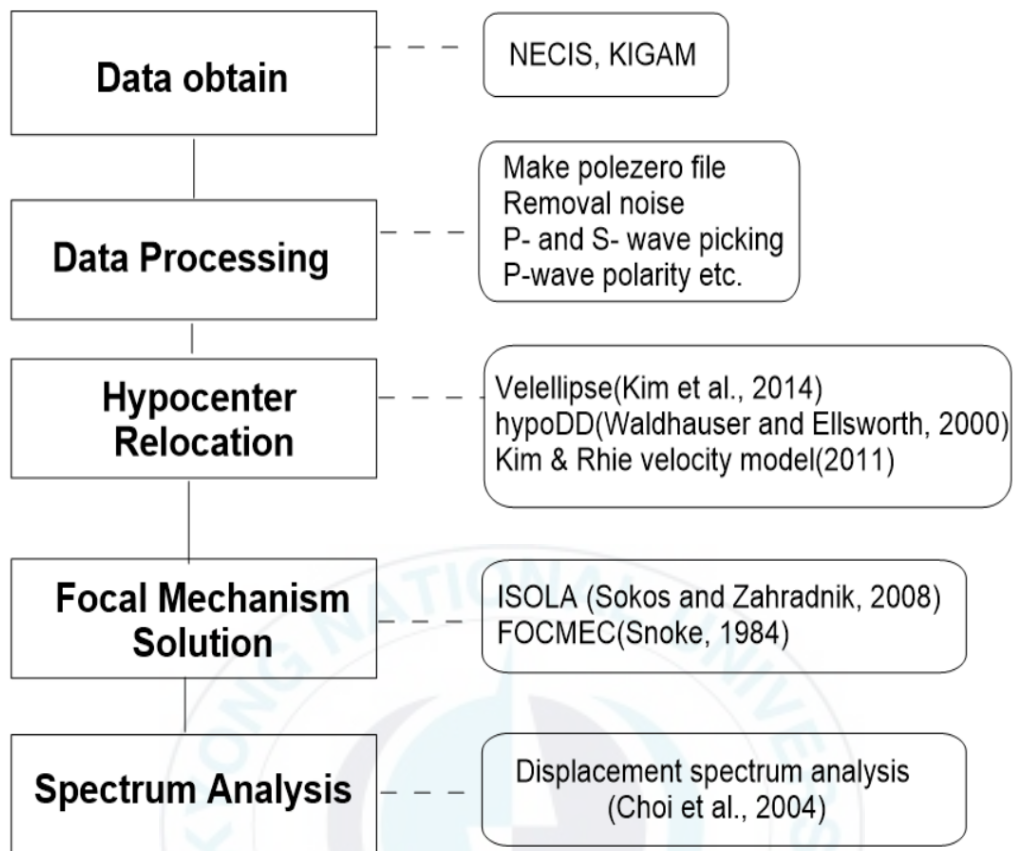
Figure 4 A work flow chart from the seismic data acquisition to get source parameters, Kim &Rhie velocity model is used in the hypocenter relocation, focal mechanism analysis. The Velellipse, HypoDD, ISOLA and FOCMEC are names of software. To confirm the reliability of moment magnitude which is one of the results of ISOLA, displacement amplitude spectral analysis calculated.
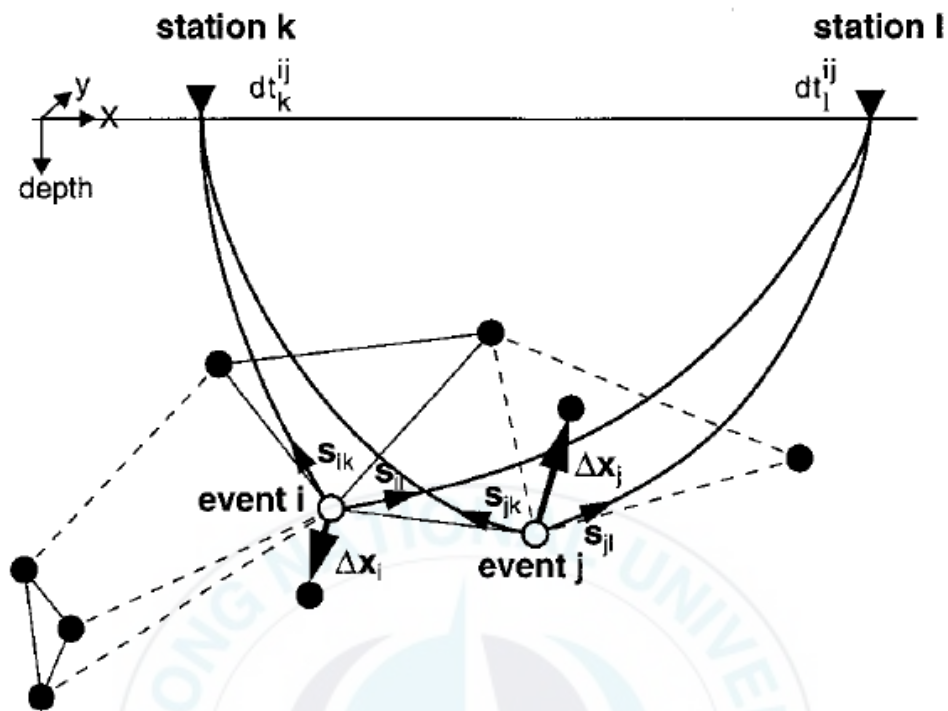
Figure 5 Illustration of the double-difference earthquake relocation algorithm. Solid and open circles represent trial hypocenters that are linked to neighboring events by cross-correlation (solid lines) or catalog (dashed lines) data. For two events, i and j, the initial locations (open circles) and corresponding slowness vectors, s, with respect to two stations, k and l, are shown. Ray paths from the sources to the stations are indicated. Thick arrows (Δ**x**) indicate the relocation vector for events i and j obtained from the full set of equation (4), and dt is the traveltime difference between the events i and j observed at station k and l, respectively (Waldhauser and Ellsworth, 2000).
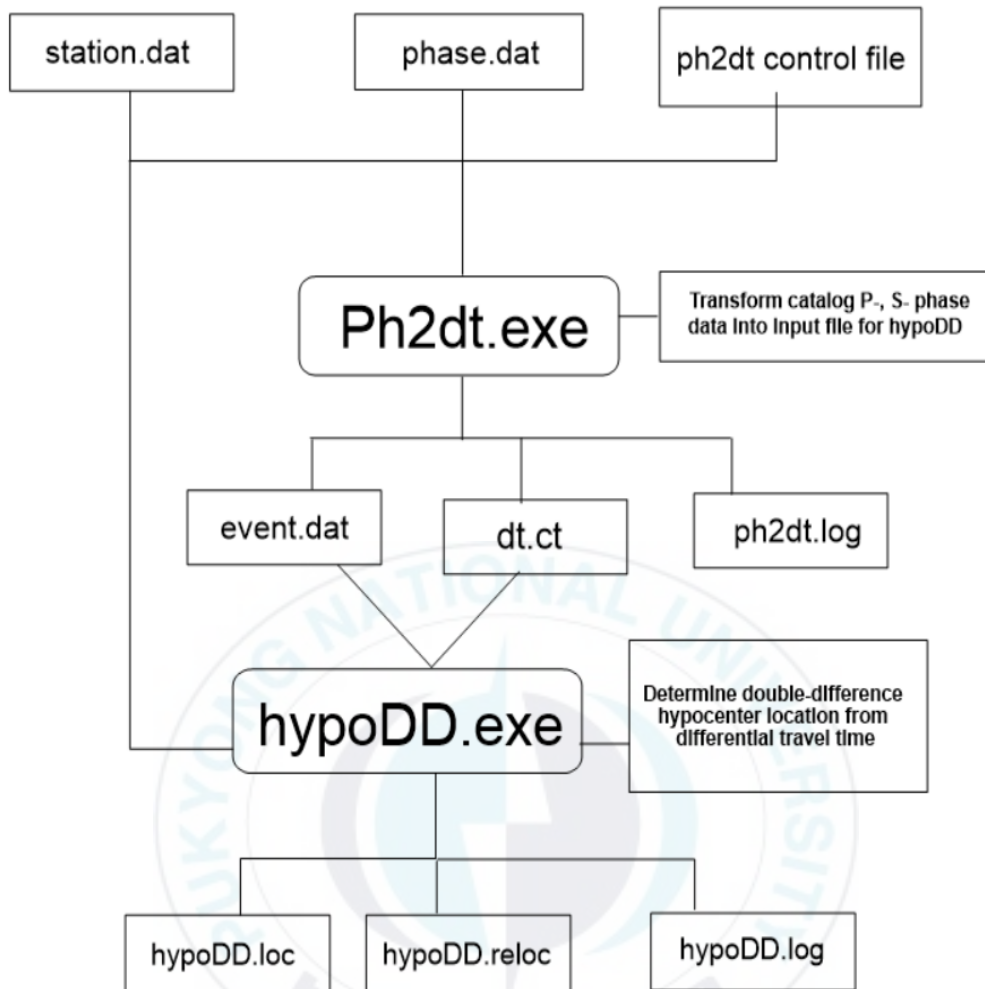
Figure 6 Event relocation with HypoDD is a two-step process. Ph2dt performs transform catalog P-, S- phase data into input files for hypoDD. HypoDD performs determine double-difference hypocenter location from differential traveltime.
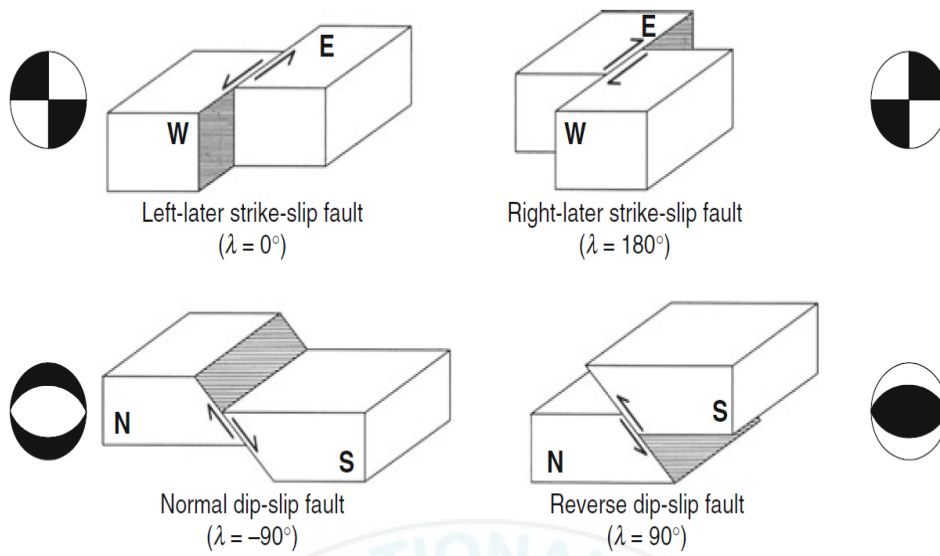
Figure 7 Examples of the most common type of focal geometries with corresponding focal mechanism patterns. (James, 1989)
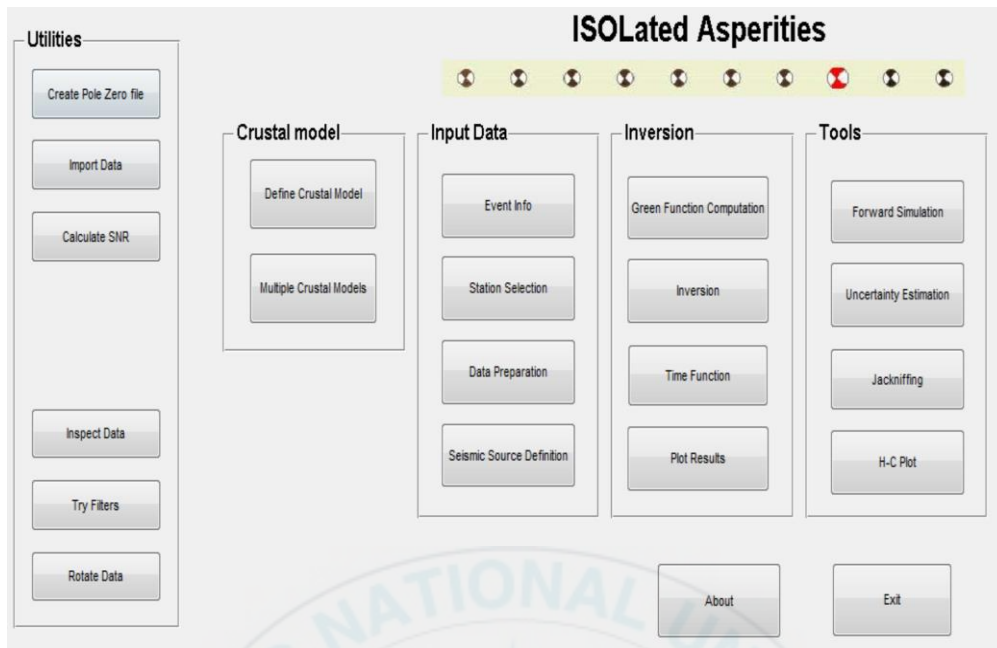
Figure 8 A ISOLA-GUI starting screen, a tip is given to the user for ease of use.
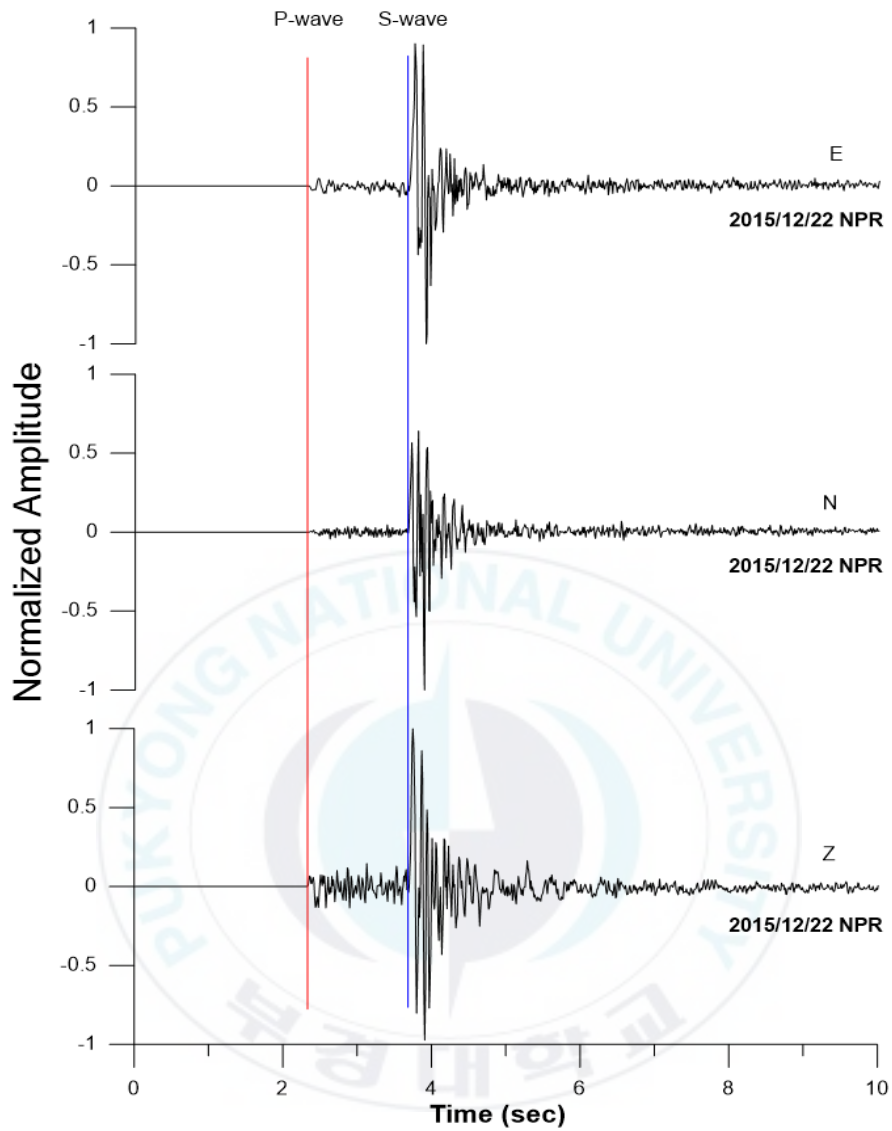
Figure 9 The normalized velocity waveforms recorded at NPR seismic station. The arrival time picks of P- and S- waves are represented by red and blue solid lines, respectively.

III Results

1. Hypocenter Relocation

This study relocated six earthquakes that occurred near Iksan in 2015 to 2016 (see Table 3 and Fig. 10). Table 3 express result of events relocation that the difference KMA, KIGAM and this study are 0.5km. There is no largely change. Most of earthquakes are concentrated at depth of 10 to 15km and are located on second layer of the velocity structure model. As a result of the Velellipse, an optimum velocity model with minimum error of a traveltime was determined for each event. Figure 11 shows how the results of each event are different from the initial velocity model. The P wave has a difference of about 0.02 from the initial velocity model and S wave shows a difference about 0.01. The initial velocity model is similar to the results. The results used for relocation seems to be consistent. But, the magnitude 0.8 indicates a large difference result because the signal used for computed source relocation is not good and input data is inaccurate.

2. Focal mechanism determination

To do waveform modeling using ISOLA, input data of velocity structure information is needed. The P- and S- wave velocity and layer depth used for the analysis are based on the velocity model of Kim, S. The density is automatically calculated in ISOLA by the following equation (10):

$$\text{Density} \left({}^{g}\!/\!{}_{cm^3} \right) = 1.7 + 0.2 * \text{Vp}({}^{km}\!/\!{}_{sec^2}) \tag{10}$$

The attenuation values were applied differently depending on the depth (Kim *et al.*, 2002, Choi, 2009). Tale 4 shows that input velocity structure model for calculating waveform modeling. This study has selected a seismic station that has enough distance for calculate and has good quality observed data. Theoretically, one seismic station can get the solution, but I selected several a seismic station centered on the source for the correct results (see Fig. 12). For compare synthetic- to observation- waveform, user applied by selected filtering frequency band. The filtering frequency band is applied according to the magnitude and distance(km), Kubo et al. (2002) announced filtering range (see Table 5). (Rhie and Kim, 2010) selected an optimal passband (0.02< Hz<0.1) for most of events that local magnitude 3.5 to 5.1. (Choi and Shim, 2009) applied the passband(0.05<Hz<0.1) for local magnitude 3.7. After testing various passbands, I selected an optimal passband that best fitting between waveforms. The applied filtering band varies with the epicenter distance (see Fig. 13). Assuming a single event for the synthetic waveform calculation, fix the source position and give only the depth change to find the solution that best matches the waveform. The given depth was 0 to 37.5km and the depth step was 2.5km. 15 iteration calculations were performed. The passband was applied differently according to the epicenter distance. After selecting a broadband seismic station more than 100km from the epicenter, it carried out inversion. As a result of the inversion, the VR (Variance Reduction) was low and inversion was performed repeatedly while reselecting the seismic stations and correcting the filtering passband. After many tests, the VR value was high when the seismic station was located at a similar distance and the suitable passband was applied. So, this study carried out inversion by dividing group into A and B by epicenter distance (see Table 6). VR (%) was calculated by using Equation (5) to compare the conformity between the observed waveforms and the synthetic waveform at each seismic station. In this study compared

the VR class given by (Roumelioti *et al.*, 2008)). The A group had 82.5% grade A, and the B group had 79.8% grade B. The B group had an appropriate solution but the VR value and grade were lower than A group. Since the VR value calculates the mean value of each seismic station component, the VR value becomes smaller when the seismic station having a low VR value is included (see Fig. 14). Figure 15 shows the correlation between the observed- and the synthetic waveform and the focal mechanism according to the test depth. The color indicates the degree (%) of Double Couplet (DC). The result of inversion of group A is VR value 90% and DC value 63.9% at depth of 10.5km. The result of inversion of group B is VR value 85% and DC value 88.3% at depth of 8km. The focal mechanism of the A- and B groups can estimate the faulting direction of NE-SW or NW-SE and show the characteristics of thrust faulting. The main direction of stress that causes this faulting is direction of WNW-SES. The main compressional axis direction that causes these earthquake is the WNW-SES. Long period waveform inversions are often inapplicable to small earthquakes that predominantly have high frequency due to low signal to noise (S/N) ratios at low frequency. Therefore, the five evens except for the magnitude 3.9 event were unable to analyze the focal mechanism using waveform inversion.

Instead the P wave polarities for calculation of focal mechanism solutions of small events are applied using the FOCMEC software (see Table 7 and Fig. 16). In case of the magnitude 3.9 event, recorded data was better than other events and about 40 stations could be analyzed. However, in case of the magnitude 0.8, there were a lot of the seismic station that was not easy to judge by the naked eye because the data quality is not good. This study used acceleration data as well as velocity data. All events analyzed using FOCMEC software did not allow error values. Results of calculation of focal mechanism, in case of multiple solution, the median value is calculated and

similar value is extracted. As a result, it can show faulting direction of the NNE-SSW or NNW-SSE from the magnitude 3.9 event on December 22, 2015(Event # 1), and demonstrate the thrust faulting. The compressive stress axis inducing fault movement is in the direction of E-W. It is possible to estimate faults in the direction of NNW-SSE or NW-SE from the focal mechanism that occurred magnitude of 0.8 on December 22, 2015(Event # 2), and shows the thrust faulting. The compressive stress axis inducing fault movement is in the direction of E-W. It is possible to estimate faults in the direction of NNW-SSE or NW-SE from the focal mechanism that occurred magnitude of 1.2 on December 22, 2015(Event # 3), and shows the thrust faulting. The compressive stress axis inducing faults movement is in the direction of E-W. It is possible to estimate faults in the direction of NNW-SSE or ENE-WSW from the focal mechanism that occurred magnitude of 1.7 on December 22, 2015(Event # 4), and shows the strike-slip faulting. The compressive stress axis inducing faults movement is in the direction of NE-SW. It is possible to estimate faults in the direction of NNE-SSW or NE-SW from the focal mechanism that occurred magnitude of 1.2 on May 11, 2015(Event # 5), and shows the normal faulting. The compressive stress axis inducing faults movement is in the direction of NE-SW. It is possible to estimate faults in the direction of NE-SW from the focal mechanism that occurred magnitude of 1.3 on February 9, 2016(Event # 6), and shows the thrust faulting. The compressive stress axis inducing faults movement is in the direction of NE-SW. Figure 17 shows the focal mechanism above the redetermination location. Except for the strike-slip – and normal faulting, the thrust faulting is predominant.

A triangle diagram was created to classify the induced faults movements in Iksan on 2015 to 2016 (see Fig. 18)

3. Spectrum Analysis

The corner frequency, moment magnitude and stress drop was obtained by spectrum analysis of the Iksan earthquake of M_L 3.9. The moment magnitude obtained from each seismic station varies according to the hypocentral distance, back azimuth, and site characteristics of each seismic station. In this study, the site characteristics of seismic station is a broadband seismic station using only STS-2 velocity seismic station. The final moment magnitude was acquired by averaging magnitudes obtained from each seismic station (Choi *et al.*, 2004, Choi, 2012). The estimated moment magnitude, corner frequency, and stress drop are 3.87 ± 0.2, 3.67 ± 1.07 Hz, and 71.83 ± 34.91 MPa, respectively (see Table 8 and Fig. 19). The moment magnitude obtained by spectral analysis is similar to that obtained by the waveform inversion analysis.

Table 3 Based on the list of source parameters announced by the KMA and KIGAM, it is result of relocation using the Velellipse software and HypoDD software.

	No.	Date	KST	Mag.(M_L)	Latitude(°N)	Longitude(°E)	Depth (Km)	RMS	Note
Origin	1	2015/12/22	04:31:25.14	4.3	36.03	126.9646	11.1	-	KIGAM
		2015/12/22	04:31:2	3.9	36.02	126.95	-	-	KMA
	2	2015/12/22	05:20:47	0.8	36.00	126.96	-	-	KMA
	3	2015/12/22	17:29:10	1.2	36.02	126.95	-	-	KMA
	4	2015/12/22	21:20:58	1.7	36.03	126.96	-	-	KMA
	5	2015/05/11	03:39:25	1.2	36.05	126.95	-	-	KMA
	6	2016/02/09	06:13:45	1.3	36.02	126.96	-	-	KMA
Velellipse	1	2015/12/22	04:31:25.192	3.9	36.0247	126.9560	9.2	0.079	-
	2	2015/12/22	05:02:59.051	0.8	36.0051	126.9633	4.08	0.0435	-

	3	2015/12/22	17:30:01.053	1.2	36.0199	126.9582	9.04	0.0624	-
	4	2015/12/22	21:21:59.184	1.7	36.0265	126.9553	10.27	0.0713	-
	5	2015/05/11	03:39:25.201	1.2	36.0562	126.9407	13.64	0.0604	-
	6	2016/02/09	06:13:45.148	1.3	36.0216	126.9446	11.32	0.044	-
HypoDD	1	2015/12/22	04:31:25.160	3.9	36.0234	126.9617	15.038	-	-
	3	2015/12/22	17:31:01.000	1.2	36.0183	126.9638	14.845	-	-
	4	2015/12/22	21:21:59.170	1.7	36.0252	126.9615	16.213	-	-
	5	2015/05/11	03:39:25.320	1.2	36.0556	126.9464	20.359	-	-

Table 4 The 1-D velocity model input to ISOLA for forward waveform modeling. P- and S-wave velocities and layer thicknesses are (Kim *et al.*, 2011). Q_P and Q_S values are Q for P- and S- waves, respectively at a reference frequency of 1 Hz based upon average crustal Q_{Lg} (1.5 Hz) ~ 714 (Chung and Lee, 2003, Chung *et al.*, 2005, Won-Young Kim, 2009).

Depth(km)	Vp(km/s)	Vs(km/s)	Rho (g/cm^3)	Q_P	Q_S
0.0	5.63	3.390	2.826	600	350
7.3	6.17	3.610	2.934	600	350
20.7	6.58	3.700	3.016	1200	700
31.3	7.77	4.440	3.254	1500	900

Table 5 Minimum epicentral distance, filter coefficients, and data length used for the inversion as a function of initial magnitude estimates provided by JMA (Kubo *et al.*, 2002)

Magnitude range	Epicentral distance (km)	Frequency range (Hz)	Data length (s)
3.5 < M <5.0	> 50	0.02 – 0.05	120
5.0 < M <6.5	> 100	0.01 – 0.05	120
6.5 < M <7.5	> 300	0.01 – 0.05	150
7.5 < M	> 600	0.005 – 0.02	180
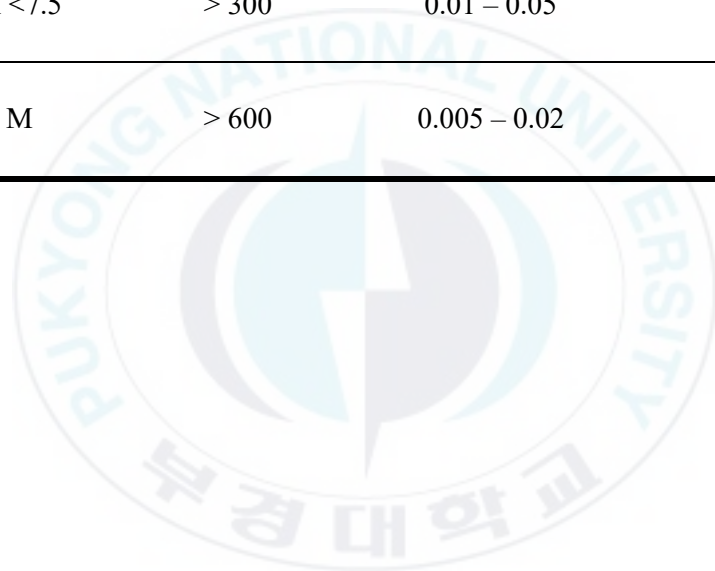
Table 6 Illustrated the waveform inversion resulting using ISOLA The results of the waveform inversion according to distance showed similar source parameters.

	A			B		
Epicenter Distance	150 ~310 km			90 ~210 km		
Moment magnitude	4.0			4.0		
Depth (km)	10.5			8		
Moment (Nm)	1.12×10^{15}			1.13×10^{15}		
VOL (%)	0.0			0.0		
DC (%)	63.9			88.3		
abs(CLVD) (%)	36.1			11.7		
Solution 1	Strike	Dip	Rake	Strike	Dip	Rake
	200	49	112	204	50	114
Solution 2	Strike	Dip	Rake	Strike	Dip	Rake
	348	46	67	350	46	64
Variance reduction (%)	82.5			79.8		

Table 7 Result of the solutions of focal mechanism by the P-wave first motion polarity analysis using FOCMEC

No.	Date	Magnitude	Strike	Dip	Rake	Strike	Dip	Rake
1	2015/12/22	3.9	351.71	48.36	62.76	209.47	48.36	117.24
2	2015/12/22	0.8	320.43	33.23	61.81	173.08	61.12	107.2
3	2015/12/22	1.2	316.65	46.03	54.04	182.91	54.37	121.33
4	2015/12/22	1.7	88.62	79.45	10.73	356.64	79.45	169.27
5	2015/05/11	1.2	243.09	39.67	-57.6	23.59	57.39	-113.96
6	2016/02/09	1.3	125.02	45.22	82.95	314.98	45.22	97.05

Table 8 The displacement amplitude spectral of the M_L 3.9 Iksan earthquake was analyzed, through the grid search method calculated moment magnitude, corner frequency and stress drop. List of result values of each seismic station that recorded the M_L 3.9 event for spectrum analysis.

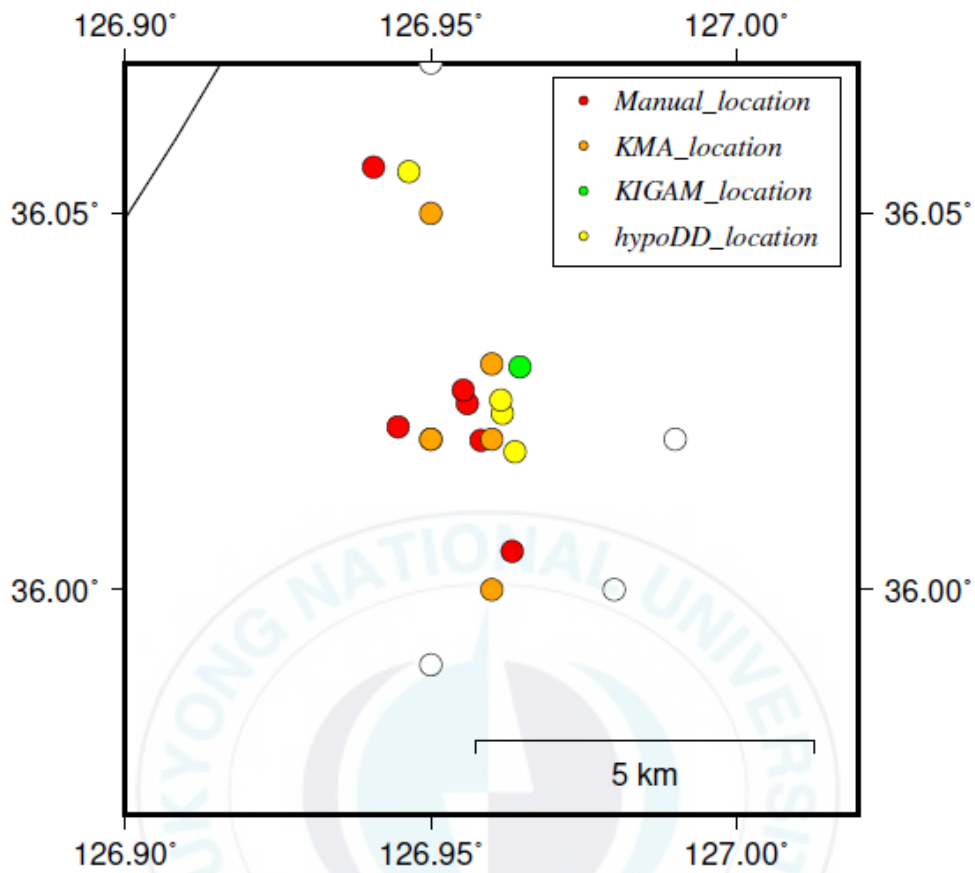| Station	Epicentral Distance (km)	M_W	F_c(Hz)	Stress drop (MPa)
TJN	53.6	3.8	2.6	19
SNU	158.3	4.0	2.3	26
HDB	223.2	3.9	3.1	46
GKP1	149.6	3.9	3.2	51
ULJ2	232.6	4.0	3.6	103
DGY2	240.1	4.0	3.3	79
DAG2	177.5	4.0	3.7	112
KWJ	96.0	3.5	5.7	72

Figure 10 Filled circles show the origin position and relocation of earthquakes near Iksan from 2015 to 2016. Orange is the event location announced by the KMA and green is the event location announced by the KIGAM. Red is the event relocation using Velellipse software and yellow is the event relocation using HypoDD software. There is no largely change.
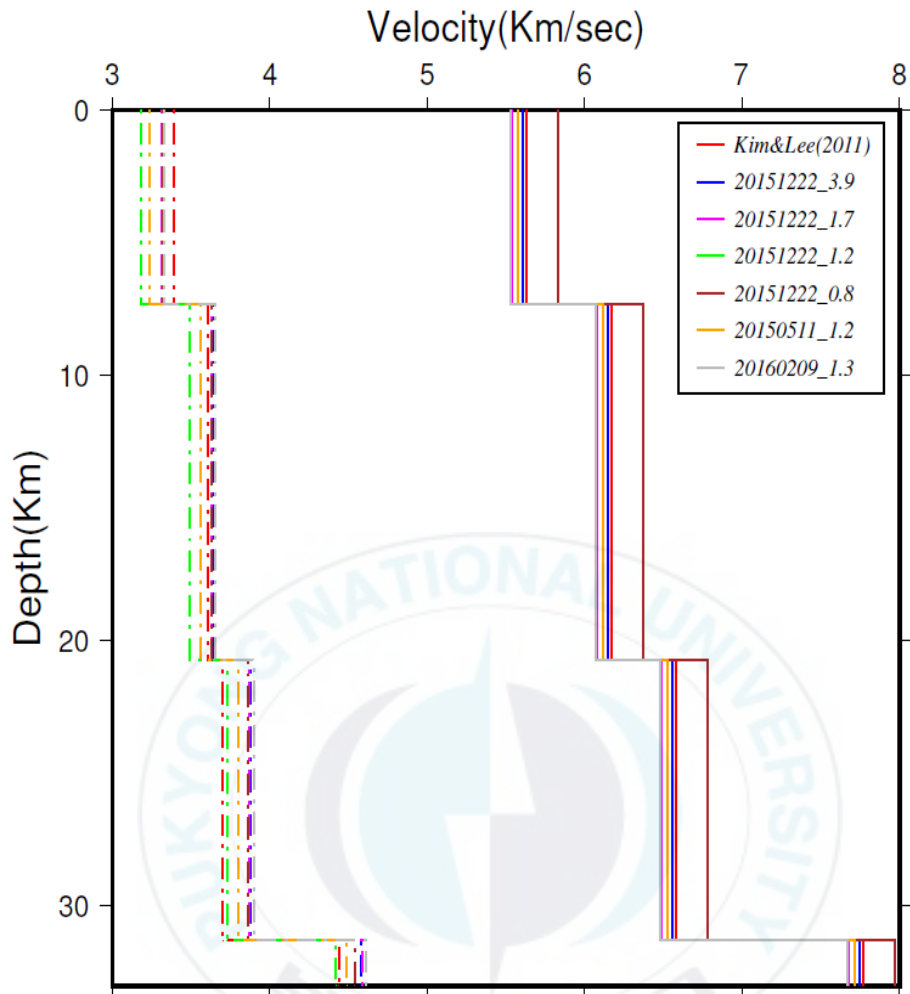
Figure 11 Presented how the results of each event are different from the initial velocity model. Red color is initial velocity model and color lines are optimum velocity model each event. The initial velocity model is similar to the results.
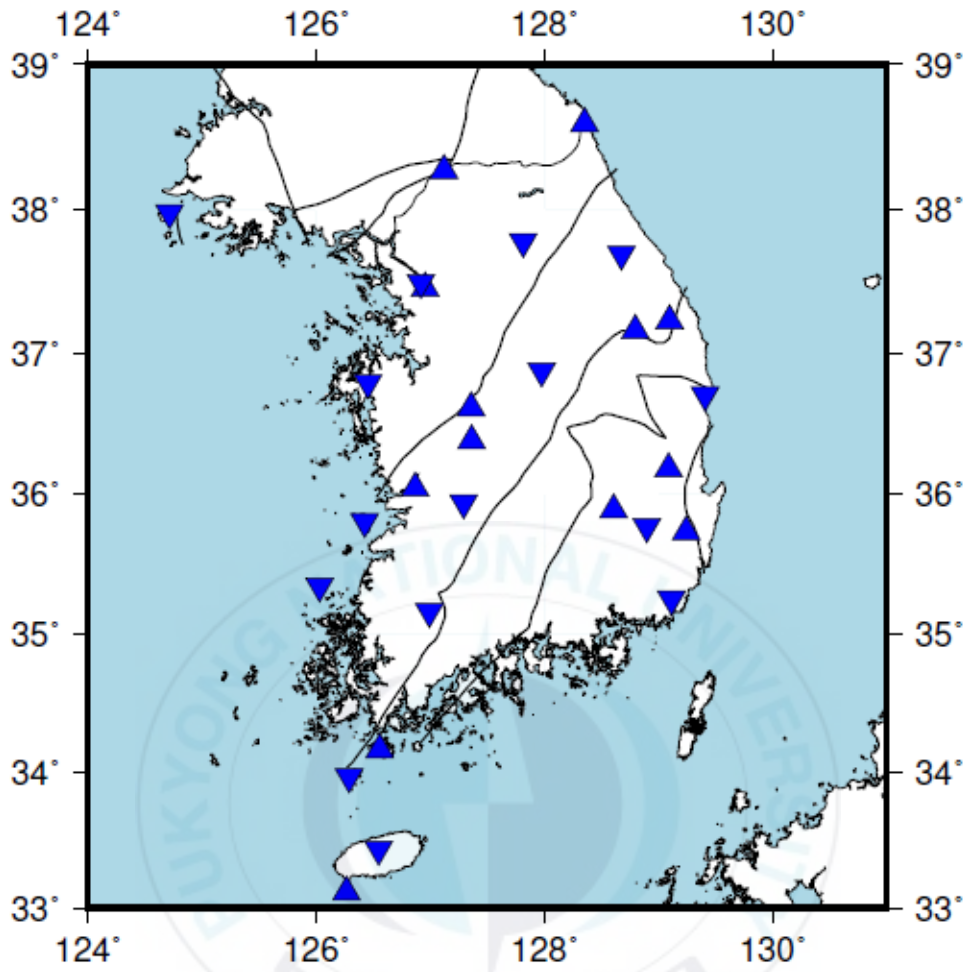
Figure 12 Location of currently operating the broadband seismic station of South Korea Reverse triangles are the broadband seismic station of KMA and triangles are broadband seismic station of KIGAM.
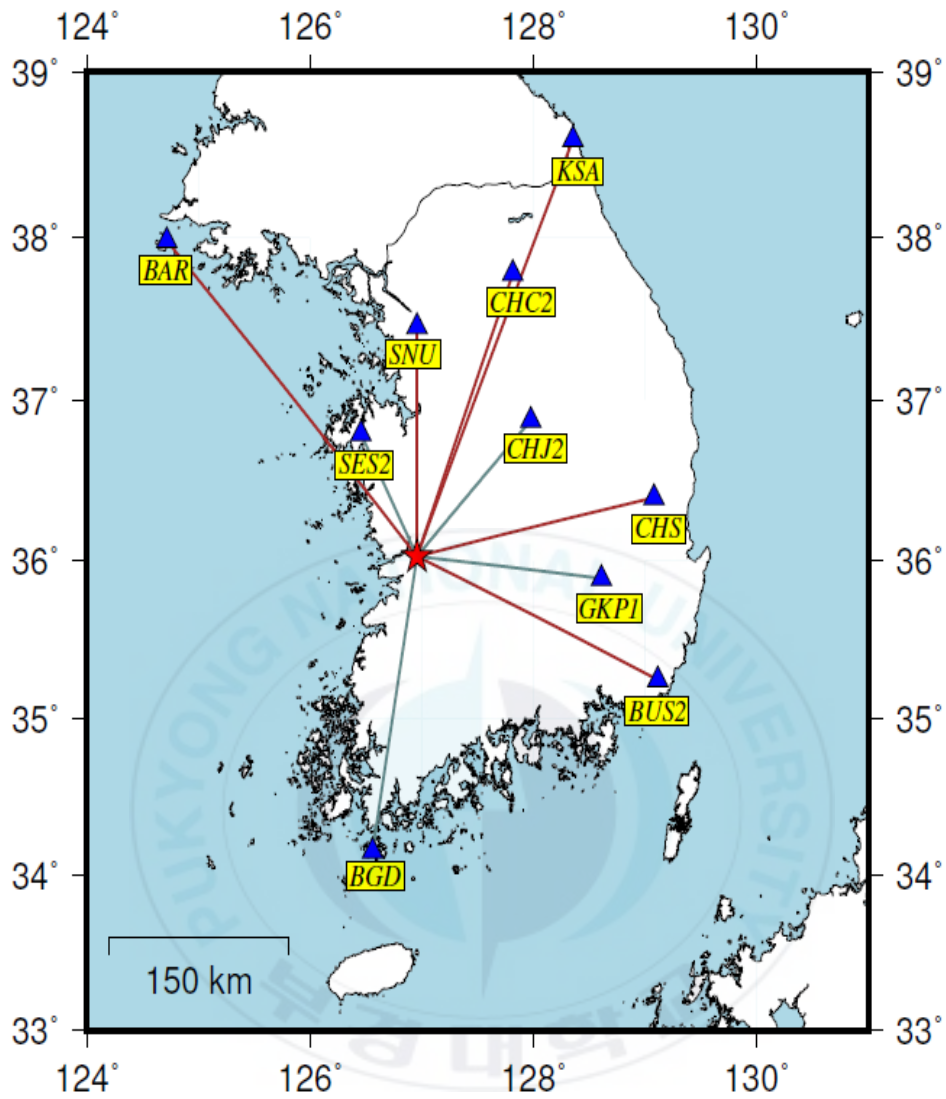
Figure 13 The applied filtering band varies with the epicenter distance. Red line (A): A group of seismic stations with an epicenter distance of 150 to 310 km. Green line (B): A group of seismic stations with an epicenter distance of 90 to 210 km.
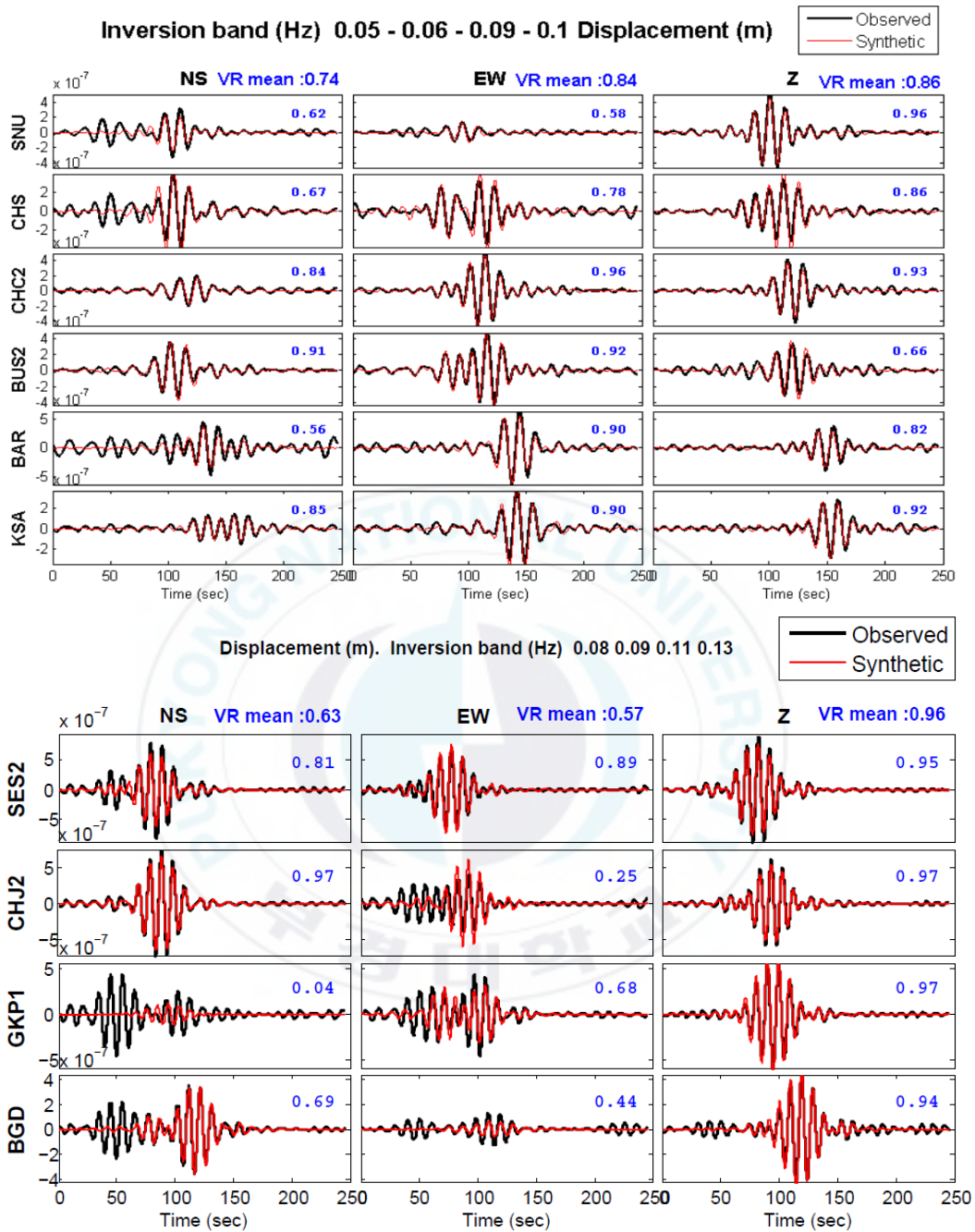
Figure 14 Analysis example of the 22 December 2015 M_L 3.9 Iksan event. The observed waveforms (black) are compared with the synthetic waveforms (red). Top was presented A group (filtering bandwidth: 0.05 to 0.1) and bottom was presented B group (filtering bandwidth: 0.08 to 0.13).
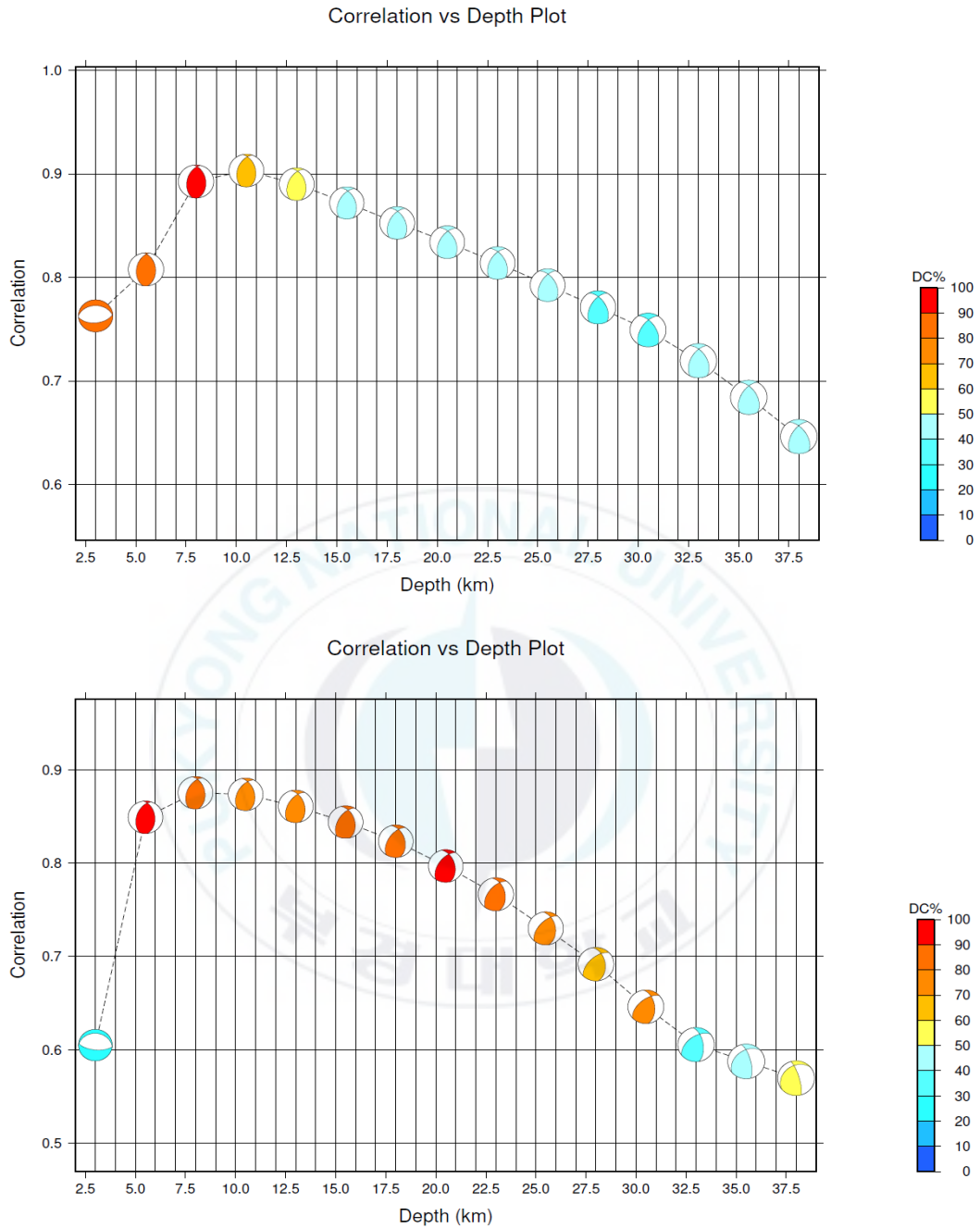
Figure 15 The variation of waveform correlations against the focal depth for the 22 December 2015 M_L 3.9 Iksan event. (Top) In case of 0.05 to 0.1 (A group) filtering bandwidth, focal depth and seismic moment are estimated to be a 10.5 km and 1.12×10^{15} Nm, respectively. (Bottom) In case of 0.08 to 0.13 (B group) filtering bandwidth, focal depth and seismic moment are estimated to be an 8 km and 1.13×10^{15} Nm, respectively.

41
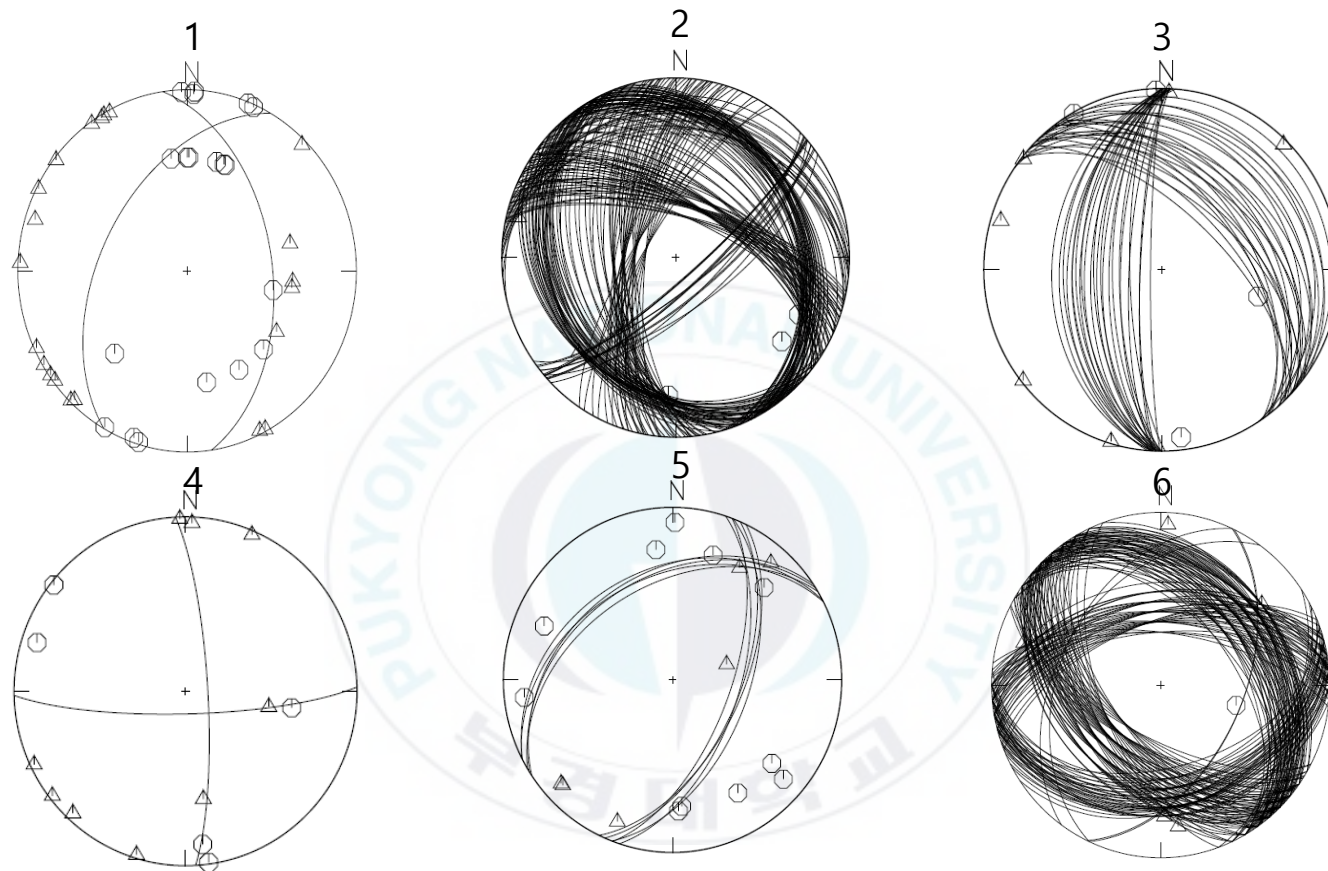
Figure 16 The determination of focal mechanism solution that occurred at 2015 to 2016 using the seismic wave polarity analysis. The data with upward (positive) P polarity area expressed with octagons, and those with downward (negative) P polarity are expressed with triangles in the focal sphere.
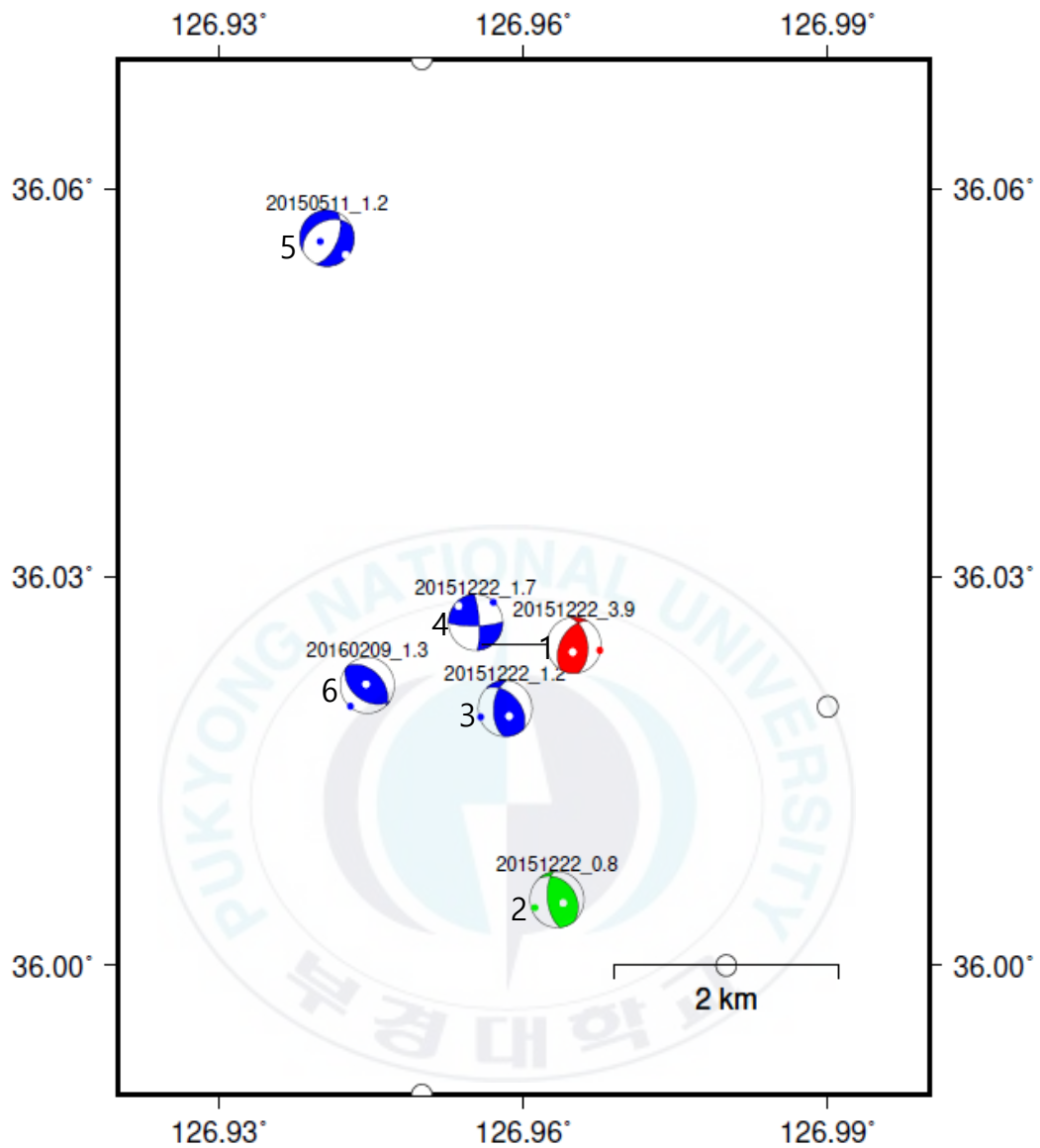
Figure 17 The 6 focal mechanism solutions of local events around Iksan. The color indicates magnitude, respectively. Red solution is M_L >3.0, blue is M_L >2.0 and green is 1 <M_L. Except for the strike-slip – and normal faulting, the thrust faulting is predominant.
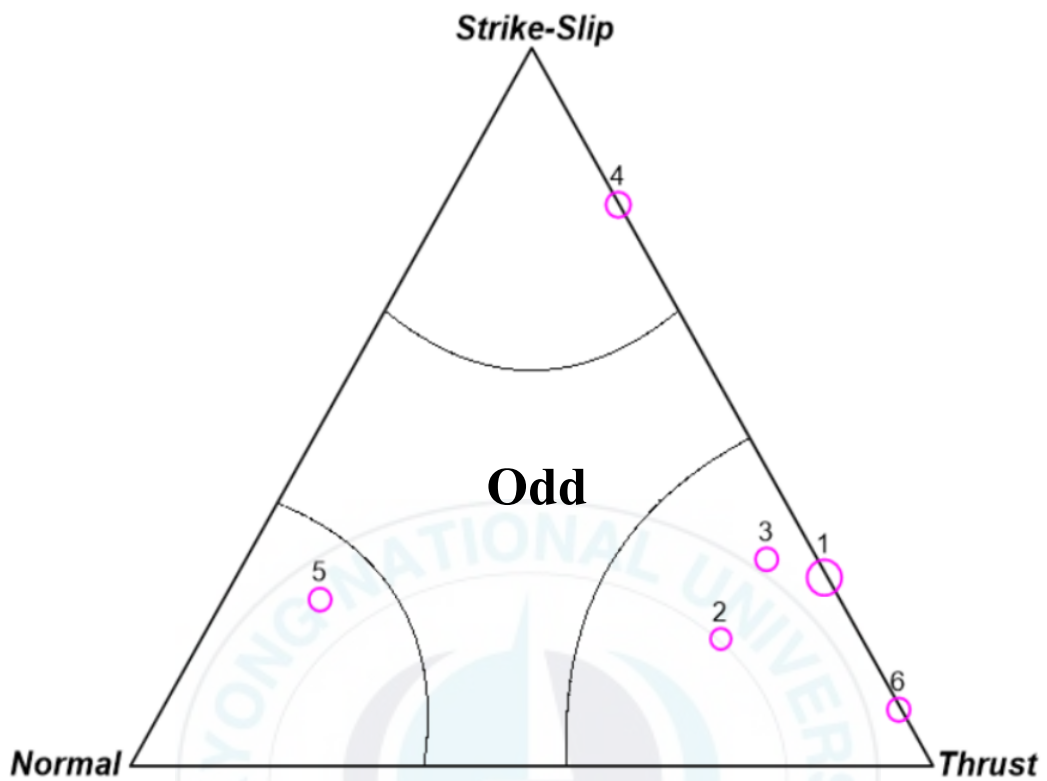
Figure 18 The event type classification of earthquakes (total 6 events) around Iksan. The dominant event type is thrust faulting earthquakes. The focal mechanism solutions of 6 events from the P polarity are plotted according to the triangle diagram (Frohlich, 1992).
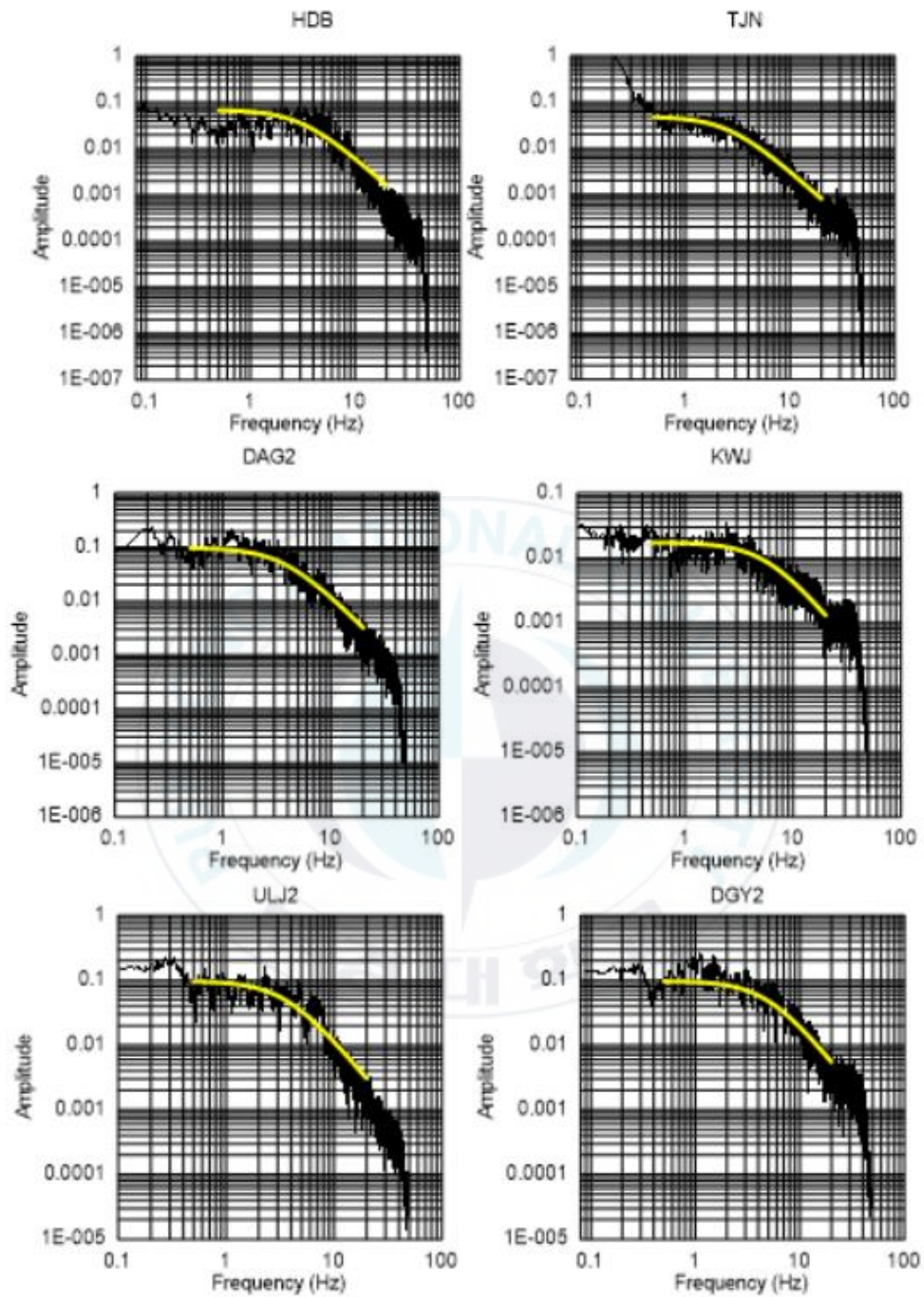
Figure 19 For the spectral analysis of the 22 December 2015 M_L **3.9** event composites Fourier amplitude spectra (thin lines) of displacements. The estimated model spectra (yellow thick lines) are superimposed.

IV Conclusions and Discussion

According to the earthquake catalog announced by NECIS, earthquakes around Iksan area from 1996 to 2016 occurred in about 20 events and the most of earthquakes were the small earthquake. Both M_L 3.6 event in 1998 and M_L 3.9 event in 2015 were that belongs to mid-magnitude level in the land shock of the South Korea. Nevertheless, Numerous former studies on source parameters are lacking in local studies called the Iksan area. This paper will help researcher to study the characteristics of the Iksan earthquake in the future. In this study, source parameters of Iksan earthquake in 2015 to 2016 were analyzed.

1. Result of events relocation that the difference KMA, KIGAM and this study are about 0.5km. There is no largely change. The KIGAM reported depth of M_L 3.9 event to be 11.1 km and this study estimated depth of occurred events in 2015 to 2016 to be 9 to 15 km. The focal depth of the Korea Peninsula earthquake is around 10km(Lee, 2010). Result of HypoDD shows that there is no correlation with the surface faulting.

2. The focal mechanism by the waveform inversion and P-wave first motion polarity analysis is that most events have thrust faulting. The compressional axes of the solutions are predominantly NE-SW in direction. This result is similar to the directions of principal compressional axes for major earthquakes occurred around South Korea (Cho *et al.*, 2006). Using the triangle diagram proposed by (Frohlich, 1992) investigated faulting type of the earthquake. Except for the strike-slip – (Event # 4) and normal faulting (Event # 5), the thrust faulting is predominant.

3. The corner frequency, moment magnitude and stress drop was obtained by spectrum analysis of the Iksan earthquake of M_L 3.9. The estimated moment magnitude, corner frequency, and stress drop are 3.87 ± 0.2, 3.67 ± 1.07 Hz, and 71.83 ± 34.91 MPa, respectively.

4. Figure 20 shows the normalized the velocity data of the vertical component of the Napoli seismic station, which recorded the earthquakes on December 22, 2015. The M_L 1.7 earthquake is different from other earthquakes. This study can confirm that the P-wave first polarity is downward. This is because the mechanism of earthquake is different, so it is considered that the focal mechanism is different.
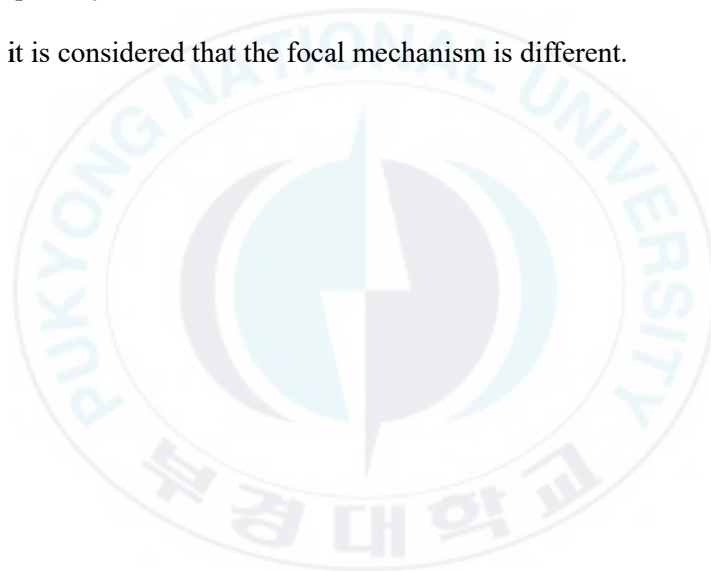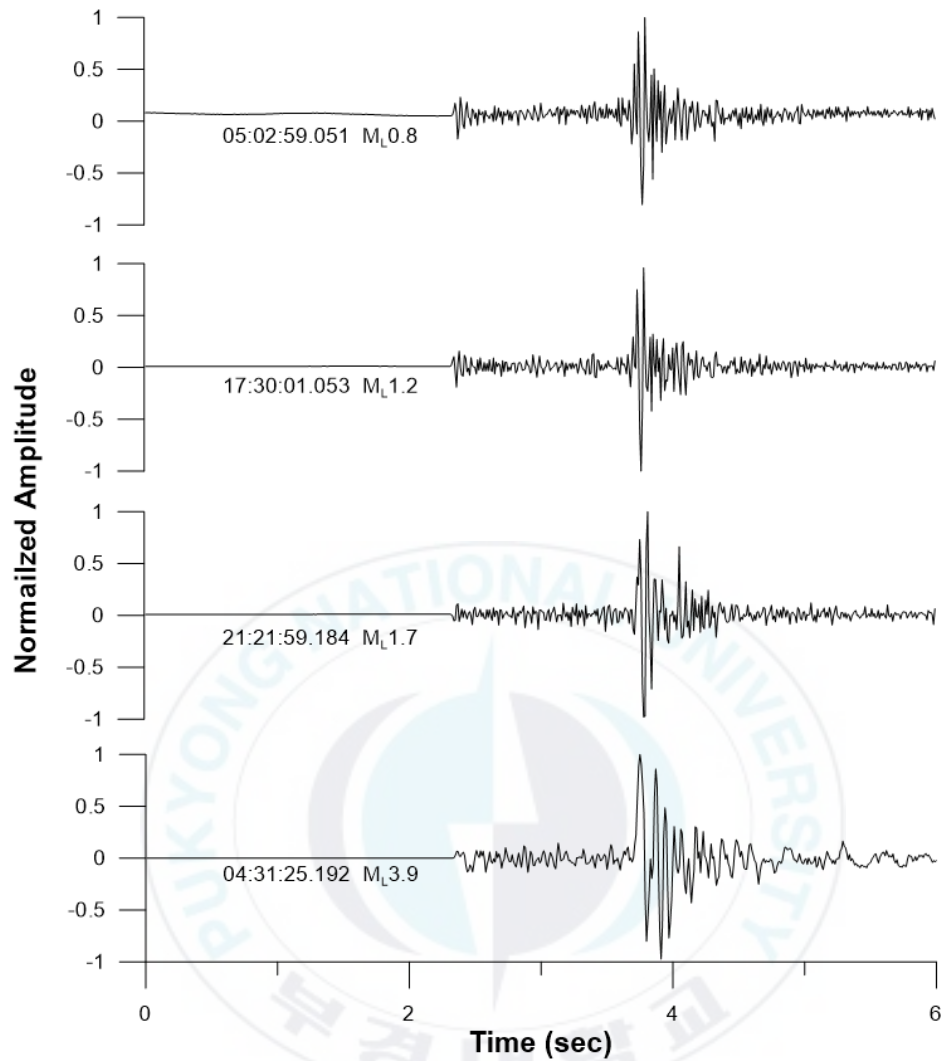
Figure 20 The normalized the velocity data of the vertical component of the Napoli seismic station, which recorded the earthquakes on December 22, 2015.

References

Bouchon, M., 1981, A simple method to calculate Green's functions for elastic layered media, Bulletin of the Seismological Society of America, 71, 959-971.

Cho, H., Kang, T. and Kyung, J., 2006, Focal mechanism solutions of microearthquakes in the Southwestern part of the Korea peninsula, Journal of the Korean earth science society, 27, 341-347.

Choi, H., Noh, M. and Choi, K., 2004, The relation between local magnitude and moment magnitude in the southern part of the Korean Peninsula, Journal of the Korean Geophysical Society, 7, 185-192.

Choi, H., 2012, Seismic characteristics of earthquakes around the Korean Peninsula and their tectonic implications. The degree of Doctor, Soul National University, Soul.

Choi, H., 2014, The Source Parameters of Offshore Earthquakes with Magnitude Larger than 4.0 Nearby Sinan, Journal of the Earthquake Engineering Society of Korea, 18, 213-219.

Choi, H., 2009, Source parameters for the December 13 1996 M L 4.5 Earthquake in Yeongwol, South Korea, Journal of the Earthquake Engineering Society of Korea, 13, 23-29.

Choi, H. and Shim, T., 2009, Analysis on the source characteristics of three earthquakes nearby the Gyeongju area of the South Korea in 1999, The Journal of Engineering Geology, 19, 509-515.

Chung, T.W., Park, Y.K. and Kang, I.B., 2005, Crustal QLg-in South Korea Using the Source Pair/Receiver Pair Method, Bulletin of the Seismological Society of America, 95, 512-520.

Chung, T. and Lee, K., 2003, A Study of High-Frequency Q (super-1) Lg in the Crust of South Korea, Bulletin of the Seismological Society of America, 93, 1401-1406.

Chung, T. and Kim, W., 2000, Fault plane solutions for the June 26, 1997 Kyong-ju Earthquake, Journal of the Korean Geophysical Society, 3, 245-250.

Cotton, F. and Coutant, O., 1997, Dynamic stress variations due to shear faults in a plane-layered medium, Geophysical Journal International, 128, 676-688.

Fréchet, J., 1985, Sismogénese et doublets sismiques. These d'Etat, Univ, Sci.Technol.Médic.Grenoble.

Frohlich, C., 1992, Triangle diagrams: ternary graphs to display similarity and diversity of earthquake focal mechanisms, Physics of the Earth and Planetary Interiors, 75, 193-198.

James, D.E., 1989, Encyclopedia of solid Earth geophysics. Springer Science & Business Media.

Jang, H.H., 2015, Analysis of correlation properties between stress drop and each earthquake source parameter. The degree of master, Pukyong National University, Busan.

Jun, M. and Jeon, J., 2010, Focal mechanism in and around the Korean Peninsula, Geophysics and Geophysical Exploration, 13, 198-202.

Jung, M.K. and Kyung, J.B., 2013, Source Characteristics of the Recent Earthquakes for Seven Years in the Southwestern Region of the Korean Peninsula, Journal of the Korean earth science society, 34, 59-68.

Kanamori, H. and Anderson, D.L., 1975, Theoretical basis of some empirical relations in seismology, Bulletin of the Seismological Society of America, 65, 1073-1095.

Kikuchi, M. and Kanamori, H., 1991, Inversion of complex body waves—III, Bulletin of the Seismological Society of America, 81, 2335-2350.

Kim, S., Rhie, J. and Kim, G., 2011, Forward waveform modelling procedure for 1-D crustal velocity structure and its application to the southern Korean Peninsula, Geophysical Journal International, 185, 453-468.

Kim, S., Kim, S. and Chi, H., 2002, Attenuation of peak spectral amplitude of acceleration in the southern part of the Korean Peninsula, Journal of Geological Society of Korea, 38, 237-250.

Kim, S., Jun, M. and Jeon, J., 2006, Recent research for the seismic activities and crustal velocity structure, Economic and Environmental Geology, 39, 369-384.

Kim, S. and Kim, B., 2008, The Seismic Source Parameters for Earthquakes Occurring in the Korean Peninsula, Journal of the Korean Earth Science Society, 29, 117-127.

Kim, W., Hahm, I., Ahn, S.J. and Lim, D.H., 2006, Determining hypocentral parameters for local earthquakes in 1-D using a genetic algorithm, Geophysical Journal International, 166, 590-600.

Kim, W., Hong, T. and Kang, T., 2014, Hypocentral parameter inversion for regions with poorly known velocity structures, Tectonophysics, 627, 182-192.

Kubo, A., Fukuyama, E., Kawai, H. and Nonomura, K., 2002, NIED seismic moment tensor catalogue for regional earthquakes around Japan: quality test and application, Tectonophysics, 356, 23-48.

Lee, K., 2010, Comments on seismicity and crustal structure of the Korean peninsula, Geophysics and Geophysical Exploration, 13, 256-267.

Noh, M., Choi, K. and Kim, T., 2003, Analysis of Fourier amplitude spectrum by composing 3-component seismic records, Journal of the Korean Geophysical Society, 6, 25-29.

Park, J., Kim, W., Chung, T.W., Baag, C. and Ree, J., 2007, Focal mechanisms of recent earthquakes in the southern Korean Peninsula, Geophysical Journal International, 169, 1103-1114.

Rhie, J. and Kim, S., 2010, Regional moment tensor determination in the southern Korean Peninsula, Geosciences Journal, 14, 329-333.

Roumelioti, Z., Benetatos, C., Kiratzi, A. and Dreger, D., 2008, Near-Real Time Moment Tensors for Earthquakes in Greece provided by the Dept of Geophysics, Aristotle University of Thessaloniki (AUTH–solutions).

Snoke, J.A., 2003, 85.12 FOCMEC: FOCal MEChanism determinations, International Geophysics, 81, 1629-1630.

Sokos, E.N. and Zahradnik, J., 2008, ISOLA a Fortran code and a Matlab GUI to perform multiple-point source inversion of seismic data, Computers & Geosciences, 34, 967-977.

Sokos, E. and Zahradník, J., 2013, Evaluating centroid-moment-tensor uncertainty in the new version of ISOLA software, Seismological Research Letters, 84, 656-665.

Waldhauser, F., 2001, HypoDD-A program to compute double-difference hypocenter locations.

Waldhauser, F. and Ellsworth, W.L., 2000, A double-difference earthquake location algorithm: Method and application to the northern Hayward fault, California, Bulletin of the Seismological Society of America, 90, 1353-1368.

Won-Young Kim, 2009, Study on Techniques for Identifying Characteristics of seismic Sources in Korea, Final Report to Korea Institute of Nuclear Safety, KINS CU08-8016, 1-111.

2015년 12월 22일 익산지진의 지진원 요소

김령이

부경대학교 대학원 지구환경과학과

요약

2015년 12월 22일 전북 익산지역(36.02°N, 126.95°E)에서 지역규모(M_L) 3.9 지진이 발생했다. 지진발생 이후 연쇄적인 지진이($M_L < 2.0$) 3회 발생했다. 지진분석을 위해 Kim, S. 1차원 층상 지각속도구조 모델(Kim *et al.*, 2011)을 일관성 있게 적용하여 위치, 깊이, 단층면해, 규모 등을 결정했다. 위치변화는 거의 없었다. 한반도 지진의 진원 깊이가 10km 내외(Kim *et al.*, 2011)인데 위치재결정 결과 분석지진 대부분이 9-13km에 분포했다. hypoDD분석 결과 지표단층과의 연계성은 없을 것으로 판단된다. 익산지진의 지진원에서 단층 운동을 유발하는 주 압축응력의 우세한 방향은 북동-남서방향으로 남한 내 주요 지진에 대하여 알려진 주 응력장과 유사하다(Cho *et al.*, 2006). 본진의 변위 진폭 스펙트럼 분석결과 **3.9±0.1**로 파형 역산을 통해 계산한 결과 4.0과 매우 유사했다.